Voluminous magma formation for the 30-ka Aira caldera-forming eruption in SW Japan: contributions of crust-derived felsic and mafic magmas

Ayumu Nishihara[1,2,3]*, Yoshiyuki Tatsumi[4], Katsuya Kaneko[1], Jun-Ichi Kimura[2], Qing Chang[2], Nobuo Geshi[3], Takashi Miyazaki[2], Bogdan Stefanov Vaglarov[2], Hironobu Hinata[1] and Keiko Suzuki-Kamata[4]

[1]Department of Planetology, Graduate School of Science, Kobe University, Kobe, Japan, [2]Research Institute for Marine Geodynamics, Japan Agency for Marine-Earth Science and Technology (JAMSTEC), Yokosuka, Japan, [3]Research Institute of Earthquake and Volcano Geology, Geological Survey of Japan (GSJ), National Institute of Advanced Industrial Science and Technology (AIST), Tsukuba, Japan, [4]Kobe Ocean-Bottom Exploration Center (KOBEC), Kobe University, Kobe, Japan

Understanding the origin, assembly, and evolution of voluminous magma that erupts in catastrophic caldera-forming eruptions (CCFEs) is a community imperative. A CCFE of the Aira caldera at 30 ka discharged over 350 km^3 of magma, which can be grouped into petrographically and geochemically distinct types: voluminous rhyolite, small amounts of rhyodacite, and andesite magmas. To further understand the magma plumbing system of the Aira CCFE, we examined the geochemical characteristics of whole rock and plagioclase from its eruptive deposits. The trace element and $^{87}Sr/^{86}Sr$ signatures recorded in the plagioclase phenocrysts of these magmas indicate that the three magmas were originally produced by partially melting an identical source rock, which was estimated to be a mafic amphibolite with an $^{87}Sr/^{86}Sr$ signature of ~0.7055 that comprised the lower crust. Melting of mafic amphibolite produced both felsic and mafic magmas by low and high degrees of partial melting, respectively. The mafic magma assimilated uppermost crustal materials and crystallized to produce an andesite magma type. The andesitic magma consists of phenocrysts (~39 vol%) and melt with a dacitic (~70 wt% SiO_2) composition. The felsic magma mixed with ~10% of the andesite magma and crystallized, forming the rhyolite magma. The mixing between the andesite and rhyolite magmas before the Aira CCFE produced the rhyodacite magma. The 30-ka Aira CCFE magmas were generated only by melting two kinds of crustal materials with different geochemical characteristics and had geochemical variations due to different conditions of partial melting and mixing between various crustal melts. The lack of definitive evidence of the mantle component mixing with the Aira CCFE magmas suggests that the mantle-derived magmas worked only as a heat source for crustal melting.

KEYWORDS

caldera-forming eruption, Aira caldera, $^{87}Sr/^{86}Sr$, partial melting, assimilation, magma mixing, LA-ICP-MS, TIMS

1 Introduction

Catastrophic caldera-forming eruptions (CCFEs) that discharge voluminous magmas rarely occur but have cataclysmic effects on Earth's evolution. They have caused destructive pyroclastic flows and widespread ashfall, injecting chemically and microphysically active gases and aerosol particles into the atmosphere (Rampino et al., 1988; Rampino and Self, 1992; Jones et al., 2005). If these eruptions occurred today, they would cause substantial damage to the global society (Newhall et al., 2018). Therefore, it is vital to understand how voluminous magma is produced, how it forms large magma reservoirs, and what triggers the CCFEs based on geological and petrological studies targeting past CCFEs.

The production of large amounts of magma that causes CCFEs is one of the important challenges for understanding volcanic activity at calderas (Hildreth, 1981; Annen et al., 2006; Bachmann and Bergantz, 2008; de Silva, 2008). The isotopic ratios of the ejecta are important for revealing the source material of magma. The isotopic analysis of whole rock samples has been conducted at various CCFEs, and the recent advancement of microscale techniques for the measurement of isotope ratios enables us to analyze the zoning structure of isotope ratios inside crystals (e.g., Oruanui supereruption, Charlier et al., 2008; Sas et al., 2021). To unravel the complex petrogenetic processes of voluminous magmas that

have caused CCFEs (Wilson et al., 2021, and references therein), sequential changes in the isotope ratios of melt that are recorded in phenocrysts are key to tracking the assimilation and mixing processes within the magma plumbing systems (Davidson et al., 2007).

The 30-ka Aira CCFE, one of Japan's largest Quaternary eruptions, is associated with a collapse of the Aira caldera with a diameter of 20 km (Figure 1) (Matumoto, 1943; Aramaki, 1984; Smith et al., 2013). The Aira CCFE discharged over 350 km³ of magma (Geshi and Miyabuchi, 2016; Takarada et al., 2022), which was mostly a compositionally homogeneous rhyolite magma (Kurasawa et al., 1984; Tsukui and Aramaki, 1990; Arakawa et al., 1998; Geshi et al., 2020; Kuritani, 2023). However, a minor amount of dark pumice with rhyodacitic composition is sometimes found within the deposit (Tsukui and Aramaki, 1990), which has different isotopic compositions from rhyolite white pumice; $^{87}Sr/^{86}Sr$ values of dark and white pumice range from 0.70646 to 0.70788 and 0.70570 to 0.70599, respectively (Arakawa et al., 1998; Kuritani, 2023). These isotopic properties suggest that the rhyolite magma was derived by the partial melting of a crust, which had limited isotope compositions, while the magma producing the dark pumice was generated by assimilation and fractional crystallization process between the basement sedimentary rocks and basaltic parental magma or by partial melting of crustal materials that underlay
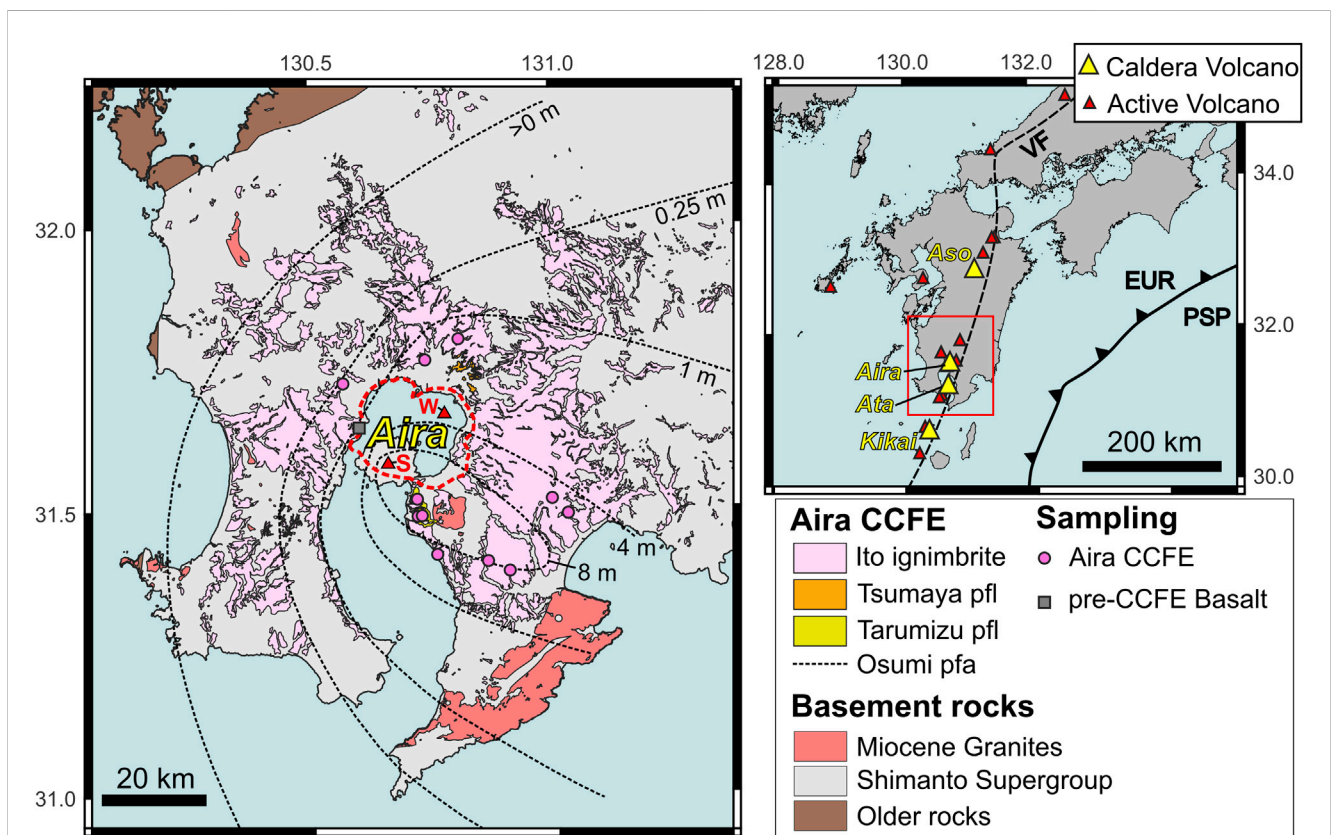
FIGURE 1
Tectonic and geological setting of the Aira caldera. The volcanoes shown in yellow in the right panel represent those that produced CCFEs over VEI-7 during the Late Pleistocene and Holocene. The dashed red line in the left panel represents the rim of the Aira caldera. The red triangles with S and W within the Aira caldera in the left panel represent the volcanic centers of the post-CCFE activities (Sakurajima and Wakamiko volcanoes, respectively). Abbreviations are given for the following features: Philippine Sea Plate (PSP); Eurasian Plate (EUR); Quaternary volcanic front (VF); pyroclastic flow deposit (pfl); pumice fall deposit (pfa).

the basement sedimentary rocks (Arakawa et al., 1998). Although it is suggested that multiple magmas, which are chemically and isotopically distinct, participated in the Aira CCFE, their formation processes and mixing relationships have not been clarified.

To further understand the magma dynamics leading to the 30-ka Aira CCFE and the genesis of the rhyolite magma, petrological and geochemical examinations, of all types of juvenile clast, are needed. In addition, the geochemical analysis of phenocrysts within the juvenile clasts would reveal hidden magma processes, e.g., what the source materials of the magmas are and how the magmas evolved prior to being discharged by the CCFE. Herein, we present the geochemical characteristics of these clasts and their phenocrysts and clarify the origin and formation processes of the three types of magmas that drove the Aira CCFE.

2 Geological background

The Aira caldera is located at the southern end of Kyushu Island in southwest Japan (Figure 1). The Sakurajima and Wakamiko volcanoes, located in the southern and northeastern parts of the Aira caldera, respectively, have been active as post-CCFE volcanic centers (Figure 1). The basement rocks around the Aira caldera consist mainly of the Shimanto Supergroup, a Cretaceous-to-Neogene subduction zone complex of oceanic and trench-fill sediments dominated by mudstone and sandstone (Wallis et al., 2020). Miocene granite rocks are also distributed in southern Kyushu Island (Figure 1).

Volcanism around the Aira caldera commenced at ~3 Ma (Kaneoka et al., 1984), and volcanic activity was concentrated during the periods 1.0–0.4 Ma and after 0.1 Ma. During 1.0–0.4 Ma, magmas with a wide range of chemical compositions, from basaltic to rhyolitic, erupted mainly as lava around the western part of the Aira caldera, although several pyroclastic eruptions also occurred (Inoue et al., 1994; Sudo et al., 2000a; Sudo et al., 2000b; Sudo et al., 2001; Kagawa and Otsuka, 2000; Nishizawa and Suzuki, 2020). After a hiatus of several hundred thousand years, during which few eruptions occurred, pre-CCFE volcanism occurred at Aira from 100 to 30 ka (Sudo et al., 2000a; Nagaoka et al., 2001). In this period, magmas of bimodal chemical compositions were discharged, i.e., mainly andesite (53–60 wt% SiO_2) and rhyolite (67–77 wt% SiO_2) compositions (Geshi et al., 2020; Kuritani, 2023).

The 30-ka Aira CCFE that created a major part of the current Aira caldera discharged >350 km³ of magma (Aramaki, 1984; Takarada et al., 2022). This event started with a Plinian eruption, which produced the Osumi pumice fall deposit (Kobayashi et al., 1983), followed by two small pyroclastic flows, Tarumizu and Tsumaya, distributed to the southeast and north of the Aira caldera, respectively (Figure 1) (Aramaki, 1969; Aramaki, 1984; Fukushima and Kobayashi, 2000; Ueno, 2016). The eruption shifted to a climatic phase, which discharged ignimbrite and its co-ignimbrite ash, called Ito ignimbrite and Aira-Tanzawa (AT) ash, respectively (Machida and Arai, 1976; Machida and Arai, 1983). The detailed eruption sequence of the Aira CCFE is described by Aramaki. (1984) and Takarada et al. (2022).

The juvenile clast type that is common to all phases of the Aira CCFE is white-colored pumice (Aramaki, 1969; 1984; Tsukui and

Aramaki, 1990). Small amounts of dark-colored pumice clasts, mingled with the white-colored pumice, are sometimes found, except in the Tsumaya pyroclastic flow deposit (Tsukui and Aramaki, 1990; Geshi and Miyabuchi, 2016; Geshi et al., 2020). Black scoria clasts are rarely found in the Osumi pumice fall deposit and Ito ignimbrite. The lithic fragments within the Aira CCFE deposits comprise mainly sedimentary and volcanic rocks (Ueno, 2007; Geshi and Miyabuchi, 2016). Granitic lithic fragments are rarely found in the Osumi pumice fall deposits (Geshi and Miyabuchi, 2016).

We collected three types of juvenile clasts (white pumice, dark pumice, and scoria) from Aira CCFE deposits. The white pumice clasts were collected from all geological units of the Aira CCFE, and the dark pumice clasts were collected from the Osumi pumice fall deposit and the Ito ignimbrite. The scoria was only collected from the Ito ignimbrite. In addition to these juvenile clasts, basaltic lava samples (Shirahama basalt; Oki and Hayasaka, 1970) that erupted in the pre-Aira CCFE period (0.48 ± 0.03 Ma; Sudo et al., 2000a) were also collected to examine the contribution of basaltic magma to the formation of voluminous magmas in the Aira CCFE. The localities for collecting the rock samples are presented in Figure 1.

3 Analytical methods

3.1 Whole-rock analyses

Whole-rock chemical compositions were analyzed using a X-ray fluorescence (XRF) spectrometer and applying the glass bead method. Rock samples were crushed into chips sized 5–10 mm and rinsed with deionized water using an ultrasonic bath. After being dried overnight, the rock chips were crushed by using a tungsten carbide mill to prepare powdered samples. The powder mixture was mixed with 1.8 g of the powdered sample, which was dried at over 100°C for 24 h, and 3.6 g of a flux (Johnson Matthey Spectroflux 100B; 80 wt% of lithium metaborate and 20 wt% of lithium tetraborate), and they were fused to make glass beads. The compositions of whole rock major elements and 10 trace elements (Cr, Ni, Cu, Zn, Rb, Sr, Y, Zr, Nb, and Ba) were determined by XRF (Rigaku ZSX Primus II) at Kobe University. Calibration lines for each element were prepared using 17 rock standards (JA-1, JA-2, JA-3, JB-1a, JB-1b, JB-2, JB-3, JF-1, JF-2, JG-1a, JG-2, JG-3, JGb-1, JP-1, JR-1, JR-2, and JR-3) from the Geological Survey of Japan (GSJ).

Based on the results of the XRF analysis, we selected four rock samples for trace element and Sr-Nd isotopic analyses; the samples had representative compositions in the three types of Aira CCFE juvenile clasts (WP:1608240602, DP:1702200203, and SC: 1702200211) and the pre-CCFE basalt (1611260501). The four selected rocks were crushed in plastic bags into chips and powdered by using a polycarbonate tube and alumina rod (a Yasui-Kikai multi-bead shocker) at the Japan Agency for Marine-Earth Science and Technology (JAMSTEC) for whole rock major and trace elements and Sr-Nd isotope ratio analyses. The trace element concentrations of the selected samples were determined by inductively coupled plasma mass spectrometry (ICP-MS) using Agilent 7500ce (Agilent Technologies, Tokyo, Japan) fitted with a PFA sample introduction and Pt-inject torch system at JAMSTEC.

The ICP-MS was operated without a collision gas and in multi-tune acquisition mode. Detailed methods, including sample digestion and instrument optimization, were described by Chang et al. (2003). The measured Eu, Gd, and Ta concentrations were corrected for oxide and hydroxide interferences. A well-established reference standard, JB-2 of GSJ, was analyzed with unknown samples. The JB-2 results obtained agreed well with the preferred values (Jochum et al., 2005), and the relative deviations were better than 5% for all rare earth elements (REEs) and other trace elements, suggesting a highly accurate and reliable analysis.

Whole rock Sr-Nd isotope ratio analysis was conducted using the methods given by Miyazaki et al. (2018). The conventional chemical separation procedures used have been described in previous studies (Takahashi et al., 2009; Hirahara et al., 2012; Miyazaki et al., 2012). The Sr-Nd separation was performed using an AG50W-X8 cation ion exchange resin (Bio-Rad, California, United States), along with Sr-spec and Ln-spec resins (Eichrom Tec. Inc., Illinois, United States). After initial separation, by using 1 mL of AG50W-X8 resin, Sr and Nd were purified using 0.05 mL of Sr-spec resin and 0.3 mL of Ln-spec resin, respectively. Column separation procedures were conducted with a fully automated open-column chemical separation system named COLUMNSPIDER, developed by JAMSTEC and HOYUTEC Co., Ltd. (Kawagoe, Japan) (Miyazaki et al., 2012). The procedural blanks for Sr and Nd were less than 37 and 1 pg, respectively. The Sr and Nd isotope ratios were measured with a thermal ionization mass spectrometer (TIMS) using a Triton TI instrument (Thermo-Finnigan (currently ThermoFisher Scientific), Bremen, Germany) at JAMSTEC. The measured Sr and Nd isotope ratios were normalized to $^{86}Sr/^{88}Sr$ = 0.1194 and $^{146}Nd/^{144}Nd$ = 0.7219, respectively, to correct for mass fractionation. The mean $^{87}Sr/^{86}Sr$ value in the standard reference materials from the National Institute of Standards and Technology (NIST) SRM 987 was 0.710244 ± 0.000019 (2SD, n = 3), and the values in the JNdi-1 standard reference materials were 0.512098 ± 0.000009 (2SE) and 0.512093 ± 0.000009 (2SE), during analytical sessions.

3.2 Phenocryst and groundmass geochemistry

The major element composition of the phenocrysts (plagioclase, pyroxene, and Fe–Ti oxides) within the mounted samples and thick sections (~500 μm thick) of three types of the Aira CCFE clasts and basalt was analyzed using JEOL JXA-8900 and JXA-8530F electron-probe micro-analyzer (EPMA) at GSJ and Kobe University. The accelerating voltage and beam current were 15 kV and 12 nA, respectively, for all elements. Probe diameters of 10 and 2 μm were used for plagioclase and the other phenocrysts, respectively, to avoid losing alkali (especially Na) elements from the plagioclase. ZAF correction procedures were employed. Relative standard deviations evaluated by international glass reference materials (SRM621 and JDF-D2) were < 1% for elements with >10 wt% (SiO_2, Al_2O_3, FeO, and CaO) and < 15% for elements with 1–10 wt% (TiO_2. MgO, K_2O, and Na_2O). Groundmass chemical compositions of the basalt were determined by using an energy-dispersive X-ray spectrometer (EDS; Oxford Instrumental X-Max 20) with a scanning electron microscope (SEM; JEOL JSM6610LV)

at GSJ, using a calibration curve method. Analytical conditions such as accelerating voltage and beam current were 15 kV and 1 nA, respectively. More detailed analytical methods and error evaluation of SEM-EDS are described in Geshi et al. (2020) and Geshi et al. (2021).

The concentrations of major and trace elements in selected plagioclase phenocrysts in the three Aira CCFE clasts and the basalt were analyzed via Laser Ablation (LA)-ICP-MS at JAMSTEC. The system comprises a 200-nm femtosecond LA coupled to a modified, high-resolution ICP-MS (Element XR, ThermoFisher Scientific, Bremen, Germany). Instrumentation and analytical protocols have been reported elsewhere (Kimura and Chang, 2012). In summary, the GSD-1G and GSE-1G synthetic glass standards of the United States Geological Survey (USGS) were applied as external calibration standards. The LA efficiency of the standards and the unknowns, as well as the signal drift, were corrected using the total normalization method (Kimura and Chang, 2012). The BCR-2G and BHVO-2G glass standards were analyzed in all sessions to confirm the analytical conditions. The same method was also applied to determine the trace element concentrations of the white pumice and scoria groundmass glasses.

The in situ Sr-isotopic composition of plagioclase was analyzed by LA-multi-collector (MC)-ICP-MS at JAMSTEC (Kimura et al., 2013; Chang et al., 2015). The identical or closely adjacent points analyzed for the trace element concentrations were carefully chosen for Sr-isotopic analysis to avoid any effects of cracks and contaminations (e.g., melt inclusions). The LA-MC-ICP-MS comprises a 193-nm excimer LA system with a COMPex 102 laser source (Coherent, Göttingen, Germany) coupled to multi-collector ICP-MS (Neptune, Thermo Fisher Scientific, Bremen, Germany) combined with an Aridus II Desolvating Nebulizer (CETAC Technologies, Omaha, United States). The laser aerosols in the He gas flow and the Aridus II solution aerosols in the Ar gas flow were mixed in a T-piece connector before reaching the ICP torch in the MC-ICP-MS. High-gain Faraday amplifiers, equipped with 10^{12}-Ω resistors (Koornneef et al., 2013), allowed all naturally occurring Sr isotopes (^{84}Sr, ^{86}Sr, ^{87}Sr, and ^{88}Sr) and ^{85}Rb to be detected. Isotopic fractionation was corrected by using a "double correction" method using natural isotope ratios of ^{84}Sr, ^{86}Sr, and ^{88}Sr stable isotope ratios. Each $^{87}Sr/^{86}Sr$ value was calculated by carefully excluding measurement times when elemental behavior and Sr isotope ratios changed systematically. The isotopically and compositionally homogeneous plagioclase crystal (MkAn; Kimura et al., 2013) was used to check the analytical condition every time. The average value of the MkAn standards was $^{87}Sr/^{86}Sr$ of 0.70343 ± 0.00025 (2SD, n = 12), which agreed with the preferred value (0.70343 ± 0.00006, 2SE) reported by Kimura et al. (2013).

4 Results

4.1 Petrography and whole rock geochemistry

Whole rock major and trace element compositions of 28 samples determined by XRF analysis in this study are listed in Supplementary
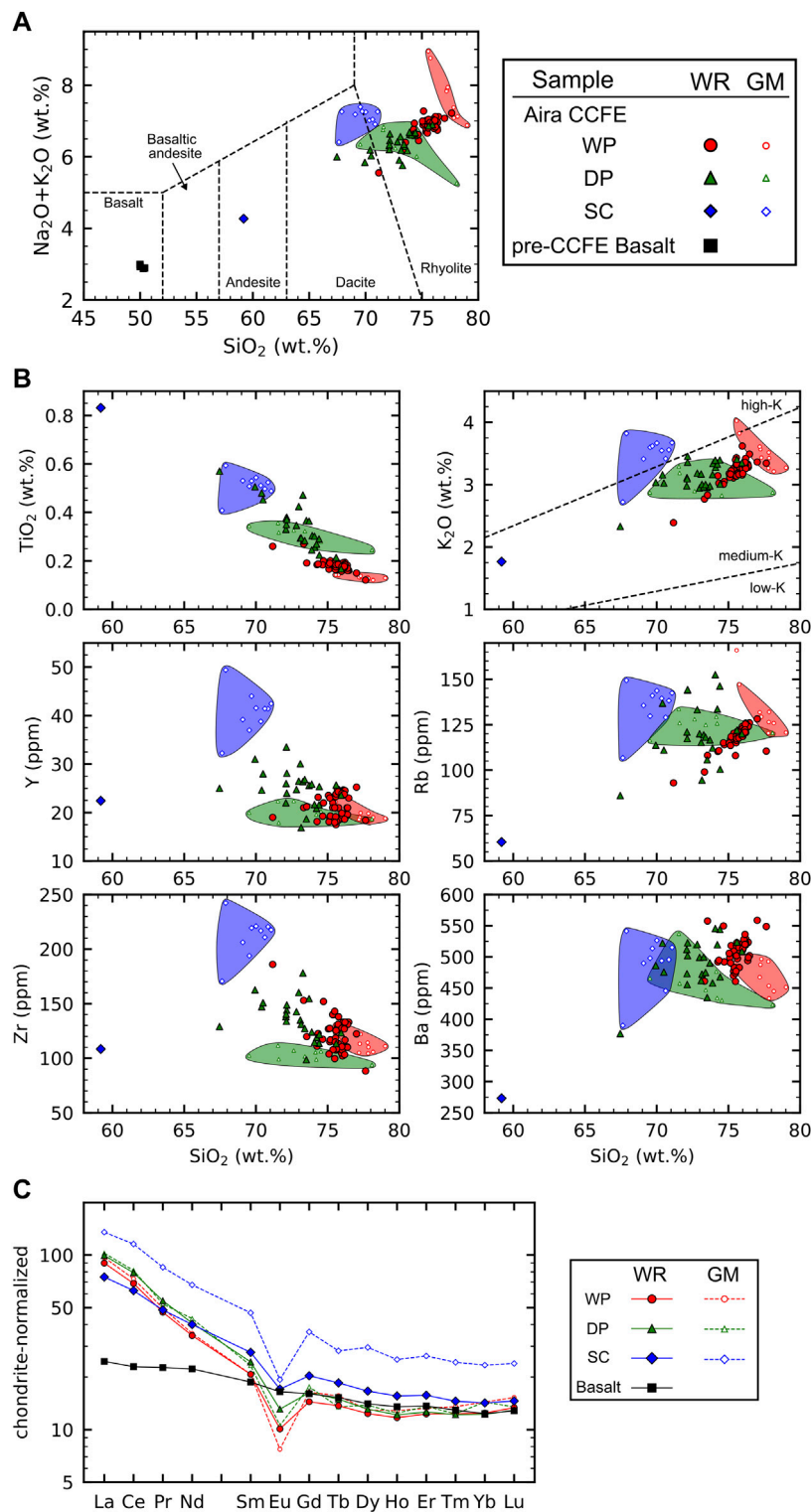
FIGURE 2
(A) TAS diagram (Le Bas et al., 1986) of the pre-CCFE basalt and the Aira CCFE clasts. Whole-rock (WR) and groundmass glass (GM) chemical variations of the pre-CCFE basalt and the Aira CCFE clasts. The 100% normalized data of WR and GM (Supplementary Tables S1, S2) are plotted, with the blue, green, and red areas representing the extent of GM composition of scoria (SC), dark pumice (DP), and white pumice (WP), respectively. The WP and DP include data from Tsukui and Aramaki (1990), Geshi et al. (2020), and Kuritani (2023). **(B)** Selected Harker diagram of the Aira CCFE clasts. The dataset and legend are the same as in Figure 2A. The classification in the K_2O diagram is based on Le Maitre et al. (2002). **(C)** Rare earth element (REE) concentrations of the selected four whole-rock data (Table 1) and average compositions of GM of the WP and SC. All data are normalized by the chondrite composition (Sun and McDonough, 1989).

TABLE 1 Geochemical and petrographical features of Aira CCFE clasts and pre-CCFE basalt.

	Aira CCFE			Basalt
Type	WP	DP	SC	Lava
Sample ID	1608240602	1702200203	1702200211	1611260501
SiO_2 (wt%)	75.5	73.5	59.2	50.3
TiO_2	0.2	0.4	0.8	0.9
Al_2O_3	13.5	14.2	17.3	18.5
FeO^*	1.6	2.7	7.7	9.7
MnO	0.1	0.1	0.2	0.2
MgO	0.3	0.9	4.1	6.4
CaO	1.9	1.9	6.3	11.1
Na_2O	3.6	3.3	2.5	2.4
K_2O	3.4	3.0	1.8	0.4
P_2O_5	0.04	0.1	0.2	0.1
XRF (ppm)				
Cr	3	21	38	36
Ni	3	8	11	19
Cu	3	6	6	34
Zn	35	42	146	86
Rb	117	116	69	9
Sr	130	144	226	349
Y	24	26	29	25
Zr	124	154	123	69
Nb	6	8	8	4
Ba	517	486	310	124
ICP-MS (ppm)				
La	21.3	23.6	17.7	5.8
Ce	42.1	48.5	38.3	14.0
Pr	4.5	5.2	4.6	2.2
Nd	16.1	19.0	18.7	10.4
Sm	3.2	3.7	4.2	2.9
Eu	0.6	0.8	1.0	1.0
Gd	3.0	3.3	4.2	3.3
Tb	0.5	0.6	0.7	0.6
Dy	3.1	3.3	4.2	3.6
Ho	0.7	0.7	0.9	0.8
Er	2.0	2.1	2.6	2.3
Tm	0.3	0.3	0.4	0.3
Yb	2.1	2.1	2.4	2.1
Lu	0.3	0.3	0.4	0.3
Hf	3.1	2.8	3.1	1.6
Ta	0.6	0.6	0.4	0.1
Tl	0.5	0.9	0.3	0.1
Pb	17.2	35.1	9.6	3.6
Th	10.3	9.9	6.0	1.0

(Continued in next column)

TABLE 1 (*Continued*) Geochemical and petrographical features of Aira CCFE clasts and pre-CCFE basalt.

	Aira CCFE			Basalt
Type	WP	DP	SC	Lava
Sample ID	1608240602	1702200203	1702200211	1611260501
U	2.3	2.0	1.3	0.2
$^{87}Sr/^{86}Sr$	0.705970	0.708558	0.707375	0.704541
2SE	0.000008	0.000008	0.000007	0.000008
$^{143}Nd/^{144}Nd$	0.512425	0.512306	0.512295	0.513100
2SE	0.000008	0.000007	0.000008	0.000006
Mineral assemblages (vol%)				
Plagioclase	10.7	5.4	25.4	31.0
Quartz	0.5	tr.	-	-
Orthopyroxene	1.4	0.3	11.8	tr.
Clinopyroxene	-	-	0.7	2.3
Olivine	-	-	-	9.3
Fe–Ti oxide	1.1	0.6	0.9	tr.
K-feldspar	-	-	-	-
Groundmass	86.3	93.7	61.2	57.2

Table S1. These and the compiled data (Tsukui and Aramaki, 1990; Arakawa et al., 1998; Geshi et al., 2020; Kuritani, 2023) are plotted on the total alkali silica (TAS) diagram (Figure 2A) and the Harker diagram (Figure 2B). The mineral assemblage and whole rock compositions of the selected four samples (three types of the Aira CCFE clasts and the pre-CCFE basalt) used for the whole rock chemical and isotopic analyses are listed in Table 1. The groundmass compositions of Aira CCFE clasts are listed in Supplementary Table S2.

White pumice (WP) and dark pumice (DP) clasts have the same phenocryst assemblages, except for DP in the Osumi pumice fall deposit: plagioclase, quartz, orthopyroxene, magnetite, and ilmenite (Table 1). The DP in the Osumi pumice fall deposit sometimes contains a small amount of K-feldspar, as well as the phenocryst minerals in the WP and the other DP. DP has fewer phenocrysts (<7 vol%) than WP (6–25 vol%) and is always mingled with WP. The black scoria (SC) clast contains abundant phenocrysts (~39 vol%) of plagioclase, orthopyroxene, clinopyroxene, ilmenite, and magnetite.

The WP clasts are rhyolitic (71–77 wt% SiO_2) in whole rock composition and are within the range of published values (Tsukui and Aramaki, 1990; Takahashi et al., 2011; Geshi et al., 2020). Little compositional difference is observed among the eruption phases, but the initial phase of the Osumi pumice fall deposit is slightly enriched in SiO_2 content (Tsukui and Aramaki, 1990). The rhyolitic WP glass compositions are homogeneous (77.4 ± 1.0 wt% SiO_2, 1SD) and are like those of the whole rock, which has the highest SiO_2 content (Figure 2A). The concentration of REEs in the WP clasts shows notable characteristics (Figure 2C). The middle REE (MREE) to
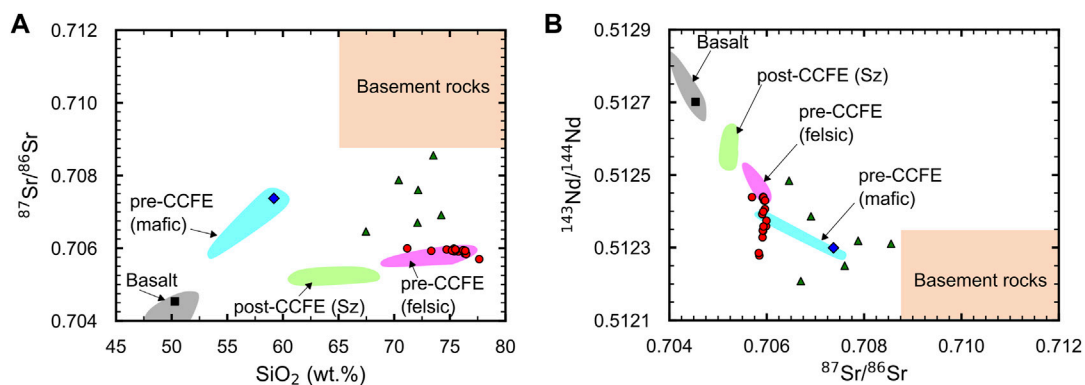
FIGURE 3
(A) Whole-rock Sr isotopic and SiO₂ and **(B)** Sr-Nd isotopic variations in the ejecta of the Aira caldera volcano. The legend is the same as Figure 2A. The WP and DP include data from Arakawa et al. (1998) and Kuritani (2023). The pre-CCFE mafic and felsic fields, the post-CCFE (Sz, Sakurajima volcano) field, the basalt field, and the basement rock field are from Terakado et al. (1988), Arakawa et al. (1998), Shinjo et al. (2000), Hosono et al. (2003), Shin (2008), Kita et al. (2012), Shibata et al. (2013), and Kuritani (2023). To ensure consistency between datasets from different institutions, all Sr and Nd isotopic data were normalized using correction factors to account for minor differences between SRM987 and JNdi-1 (or La Jolla) secondary standards measured during each study. The conversion formula for JNdi-1 and La Jolla is based on Tanaka et al. (2000).

heavy REE (HREE) concentrations of the whole rock WP are the most depleted in the Aira CCFE clasts and similar to those of the pre-CCFE basalt. This signature is also observed in the WP glass composition. The $^{87}Sr/^{86}Sr$ and $^{143}Nd/^{144}Nd$ values of the WP in whole rock are 0.705970 ± 0.000008 and 0.512425 ± 0.000008 (2SE), respectively (Table 1), which are within the ranges of published values (Arakawa et al., 1998; Kuritani, 2023).

The DP clasts show rhyodacite to rhyolite compositions (72–76 wt% SiO₂) in whole rock. Previous studies reported more SiO₂-poor DP clasts (up to 67 wt%) within the Aira CCFE deposits (Tsukui and Aramaki, 1990; Geshi et al., 2020). Most DP clasts show SiO₂ contents lower than those of the WP clasts, although some clasts enriched in SiO₂ contents overlap in chemical compositions with the WP (Figure 2A). The glass compositions of the DP also show a wide range of SiO₂ content (69.5–78.1 wt%), with similar ranges to the compositions of the whole rock. The DP clasts have different chemical trends compared to the WP clasts in the Harker diagrams, especially in incompatible elements (Figure 2B). Large-ion lithophile element (LILEs, i.e., K₂O, Rb, and Ba) concentrations in the DP do not correlate with SiO₂ content, but high-field-strength elements (HFSEs, e.g., TiO₂ and Zr) show some correlation with SiO₂ content, e.g., TiO₂ content increases as the SiO₂ content decreases (Figure 2B). These chemical trends of the DP differ from those of the WP. Furthermore, the DP clasts show different isotopic characteristics compared to the WP clasts (Figure 3). The DP has a higher $^{87}Sr/^{86}Sr$ of 0.708558 ± 0.000008 and a lower $^{143}Nd/^{144}Nd$ of 0.512306 ± 0.000007 than the WP. The DP measured in this study shows similar isotopic signature of the DP clasts reported by Arakawa et al. (1998) and Kuritani (2023) and is the most radiogenic isotopic value of the DP (Figure 3). These values show similar characteristics to those of the basement rocks (Shimanto Supergroup sediments and Miocene granites) of the Aira caldera ($^{87}Sr/^{86}Sr$ > 0.70885 and $^{143}Nd/^{144}Nd$ < 0.51234; Terakado et al., 1988; Hosono et al., 2003; Shin, 2008).

The SC shows andesitic composition (59 wt% SiO₂) in whole rock, whereas it has rhyodacitic (67–71 wt% SiO₂) groundmass

glasses. SC contains abundant incompatible elements, especially in the groundmass glasses (Figures 2B, C). The LILE and HFSE concentrations of the SC glass are similar to those of the DP with lower SiO₂ content (Figure 2B). The whole rock Sr-Nd isotope values are $^{87}Sr/^{86}Sr$ of 0.707375 ± 0.000007 and $^{143}Nd/^{144}Nd$ of 0.512295 ± 0.000008, respectively, which are similar to those of pre-CCFE mafic products (Figure 3; Kuritani, 2023).

The pre-CCFE basalt contains plagioclase, olivine, and clinopyroxene as the main phenocryst phases, with a small amount of orthopyroxene and Fe–Ti oxides. The HREE concentrations of basalt are low but higher than those of the WP, except for Yb and Lu (Figure 2C). The whole rock chemical and isotopic values of the pre-CCFE basalt are within the range of published values of basalt rocks distributed in southern Kyushu (Arakawa et al., 1998; Shinjo et al., 2000; Kita et al., 2012; Shibata et al., 2013).

4.2 Plagioclase geochemistry

Representative back-scattered electron (BSE) images of plagioclase phenocrysts within the WP, DP, and SC are displayed in Figure 4. The WP plagioclase commonly has several chemical zones (p13, q1, q2, and q3 in Figure 4), sometimes accompanied by outermost thick rims up to 200 μm (q2 and q3 in Figure 4). The WP plagioclase phenocrysts have cores that exhibit molten texture (q2 and q3 in Figure 4). The DP plagioclase phenocrysts show a similar texture to the WP (r4 in Figure 4). In contrast, the SC plagioclase phenocrysts commonly have clear cores (m153 in Figure 4).

Anorthite (An) content [An# = 100 × Ca/(Ca + Na + K)] distributions of the plagioclase within the three Aira CCFE clasts and the pre-CCFE basalt are shown in Figure 5A. In Aira CCFE clasts, the An contents of the plagioclase rims show unimodal distributions with peaks of ~An₄₀ (WP and DP) and ~An₇₇ (SC). However, the An content distribution of the plagioclase cores differs
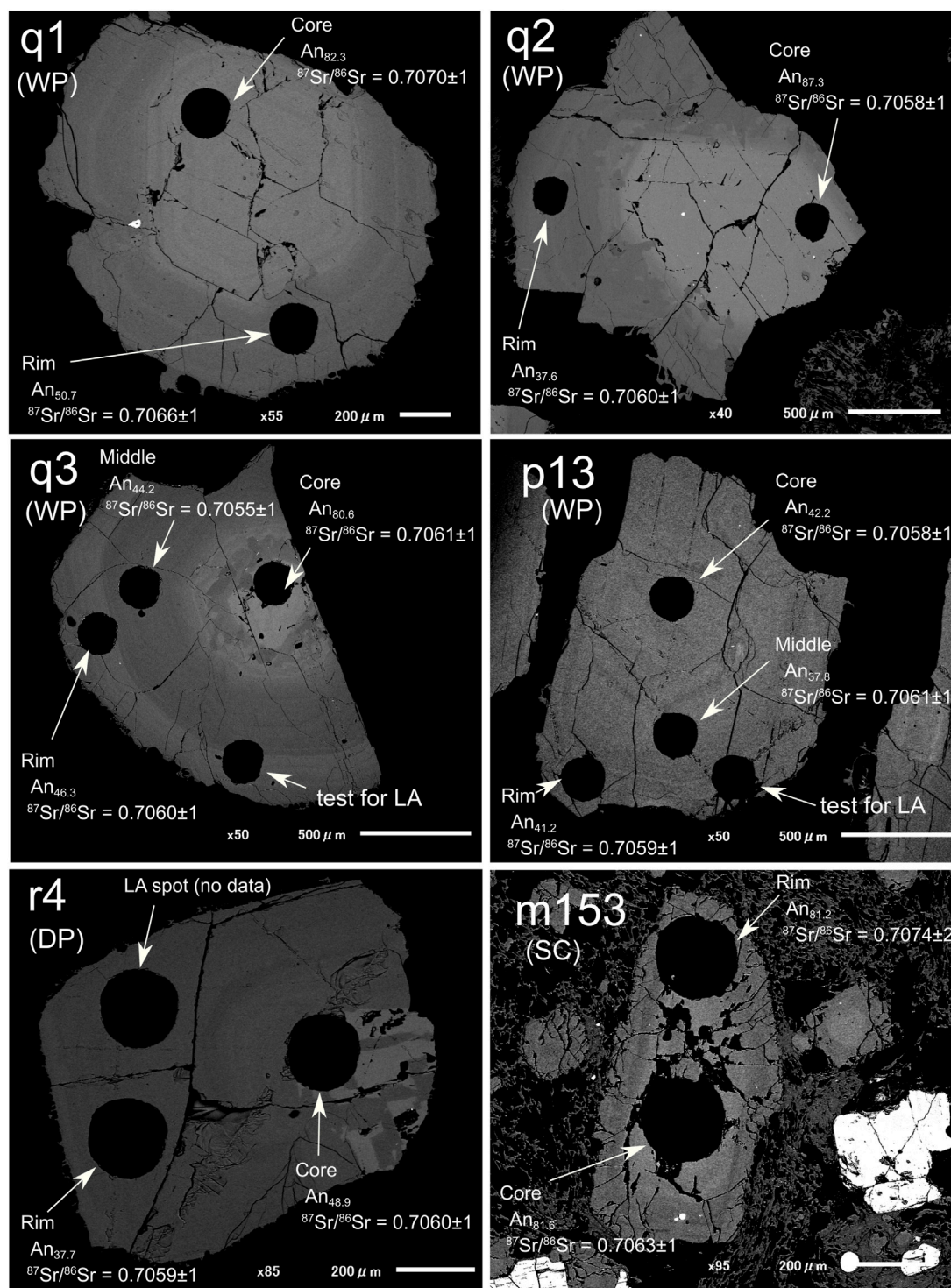
FIGURE 4
Representative BSE images of plagioclase phenocrysts within the Aira CCFE clasts. The q1, q2, q3, and p13 plagioclase phenocrysts are contained within the WP. The r4 and m153 plagioclase phenocrysts are within the DP and SC, respectively.

among WP, DP, and SC. The WP and DP have bimodal An-distributions in cores, most of them show low An ($<An_{64}$) contents with a peak of An_{43} and An_{39}, respectively, and small numbers of cores with high An ($>An_{64}$) contents, whereas the SC has high-An# cores (An_{66-91}) (Figure 5A). The An contents of the

plagioclase within the pre-CCFE basalt have higher-An cores with a peak of An_{91} than those in the SC. Figure 5B shows trace element concentrations within the plagioclase, suggesting that the nature of high-An plagioclase within the Aira CCFE clasts and the pre-CCFE basalt is different.
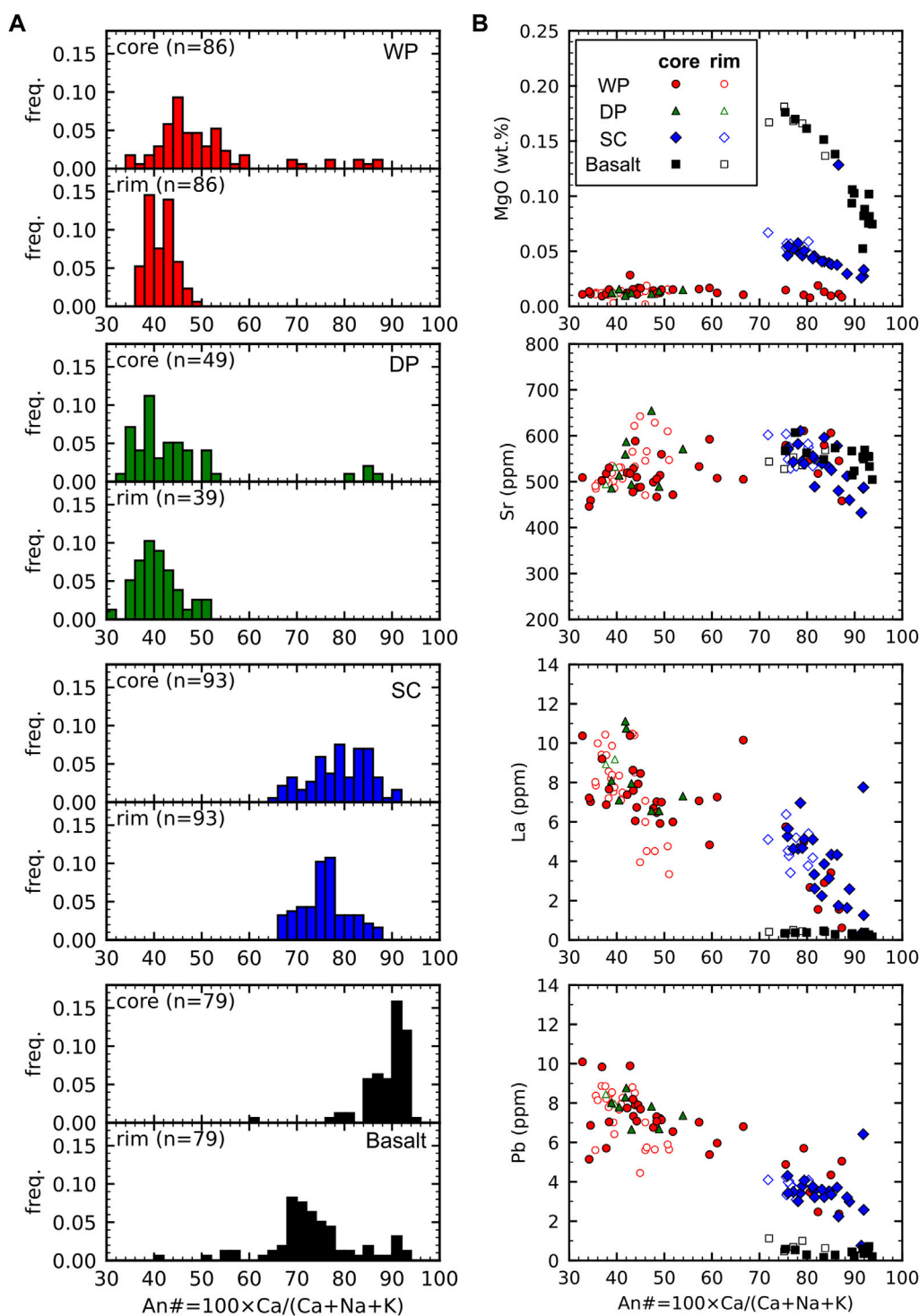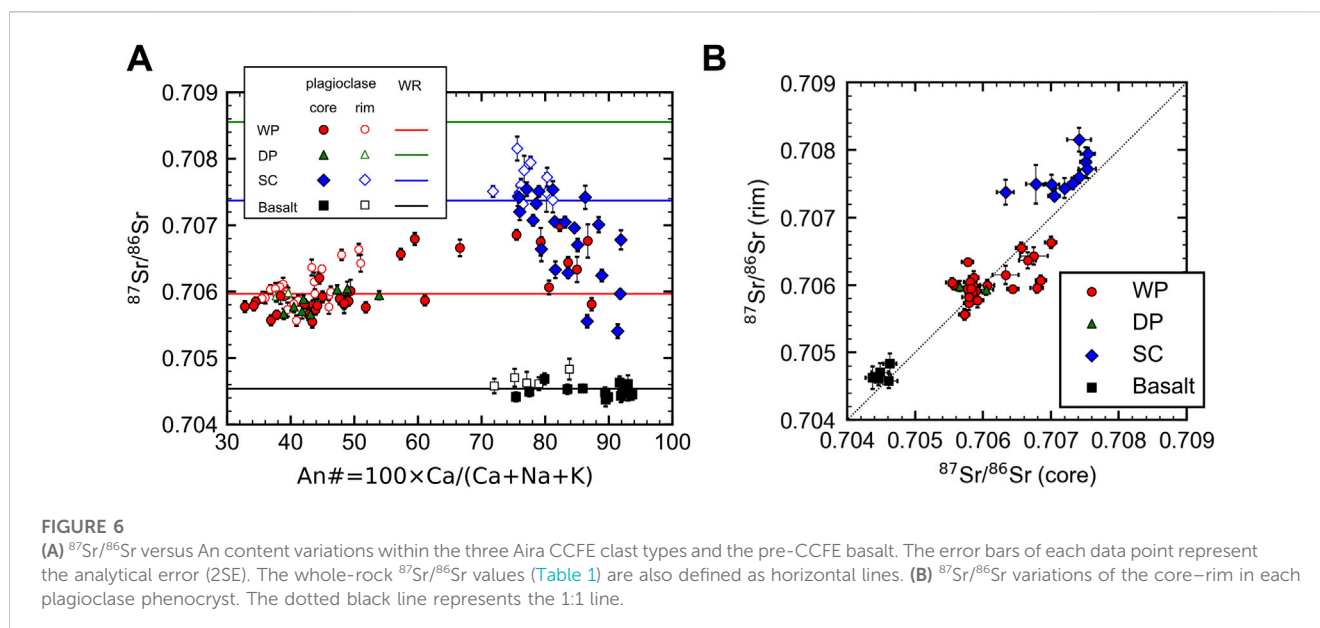
FIGURE 5
(A) Relative frequency (freq.) distributions of the anorthite (An) values (An#) of plagioclase phenocrysts within each of the Aira CCFE clast types and the pre-CCFE basalt determined by EPMA. The upper and lower panels represent the core and rim parts of the plagioclase, respectively. The vertical axis shows the relative frequency of plagioclase analyses for each sample type (core and rim). **(B)** Trace element concentrations of plagioclase phenocrysts determined by LA-ICP-MS.

Sr isotope ratios ($^{87}Sr/^{86}Sr$) versus An# variations in plagioclase are shown in Figure 6A, accompanied by the whole rock $^{87}Sr/^{86}Sr$ values. Critically, the lowest $^{87}Sr/^{86}Sr$ values within the WP and SC are identical regardless of the An content and are higher than those

of the pre-CCFE basalt (Figure 6A). In the WP, the $^{87}Sr/^{86}Sr$ values of the lower-An plagioclase core (<An$_{50}$) show a narrow range of 0.7055–0.7062, and those of the plagioclase with An$_{50-87}$ are constant or increase (0.7058–0.7070) as the An contents of

FIGURE 6
(A) $^{87}Sr/^{86}Sr$ versus An content variations within the three Aira CCFE clast types and the pre-CCFE basalt. The error bars of each data point represent the analytical error (2SE). The whole-rock $^{87}Sr/^{86}Sr$ values (Table 1) are also defined as horizontal lines. **(B)** $^{87}Sr/^{86}Sr$ variations of the core–rim in each plagioclase phenocryst. The dotted black line represents the 1:1 line.

plagioclase increase (Figure 6A). In contrast, the $^{87}Sr/^{86}Sr$ values of plagioclase within the SC increase (0.7054–0.7075) as their An contents decrease (An_{92} to An_{75}). The average $^{87}Sr/^{86}Sr$ value of the plagioclase rim within the SC is 0.7076 ± 0.0005 (2SD), which is similar to the whole rock $^{87}Sr/^{86}Sr$ value (0.7074) of the SC. The $^{87}Sr/^{86}Sr$ values of the plagioclase within the DP are 0.7056–0.7060, similar to those of the WP, but different from the whole rock values (0.7086), suggesting that the plagioclase within the DP are xenocrysts of the WP magma. The pre-CCFE basalt contains plagioclase with low $^{87}Sr/^{86}Sr$ values (0.7044–0.7047), in common with the whole rock characteristics. All analytical results of the plagioclase by LA-ICP-MS are listed in Supplementary Table S3.

In each plagioclase crystal within the SC, the $^{87}Sr/^{86}Sr$ value of the rim tends to be higher than that of the core (Figure 6B). For the m153 plagioclase within the SC (Figure 4), the $^{87}Sr/^{86}Sr$ values are 0.7063 and 0.7074 in the core and rim, respectively. In contrast, the plagioclase in the WP shows plagioclase with both higher and lower $^{87}Sr/^{86}Sr$ values in the rim than in the core. In q1 and q2 plagioclase with the high-An core (Figure 4), the $^{87}Sr/^{86}Sr$ values in q1 decrease from the core (0.7070) to the rim (0.7066), whereas those in q2 are similar in the core (0.7058) and the rim (0.7060). In q3 plagioclase, the $^{87}Sr/^{86}Sr$ values from the core to the mantle covering it (the middle region in Supplementary Table S3) decrease slightly (0.7061–0.7055), but that in the outermost rim (0.7060) increases again. For the plagioclase with the low-An core within the WP, the $^{87}Sr/^{86}Sr$ values from the core to rim regions remain unchanged or increase slightly (e.g., p13 in Figure 4).

4.3 Other phenocryst geochemistry, temperature, and oxygen fugacity

In this study, no unified thermometer can be applied to estimate the temperature of magma due to differences in the phenocrysts contained within the different clast types. Since a temperature assumption is necessary to calculate the elemental partition coefficie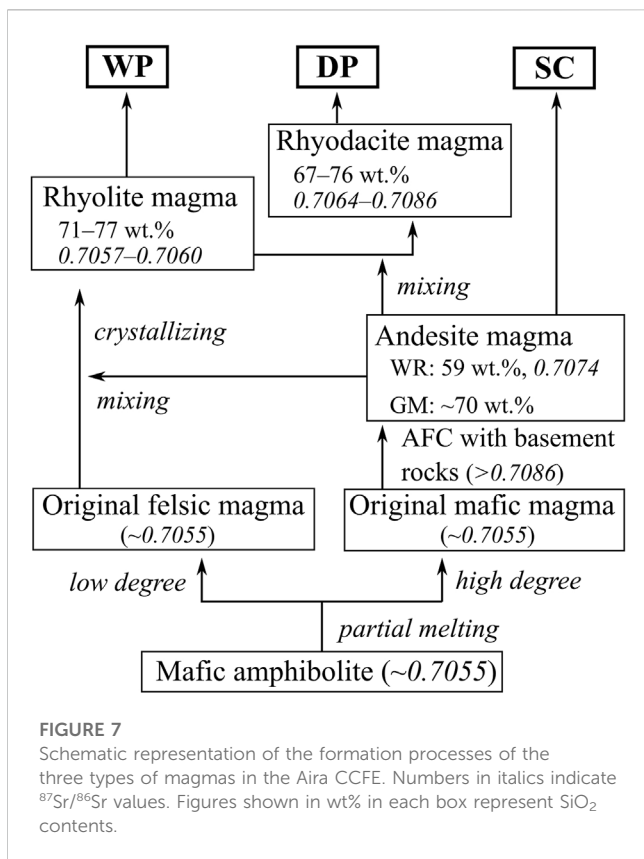nts between plagioclase and melt, the temperature of each magma type was estimated here using several available thermometers.

The temperature-fO_2 characteristics of Aira CCFE clasts based on Fe–Ti oxides (Ghiorso and Evans, 2008) are shown in Supplementary Figure S1. Because we could not find magnetite and ilmenite pairs in contact within the DP and SC, we measured the chemical composition of individual minerals in the thin section and then, by using every combination of the measured value, plotted the data for (non-touching) pairs that satisfied the requirements for equilibrium (Bacon and Hirschmann, 1988). The temperatures of WP and DP are estimated at ~800°C (792°C ± 15°C, 1SD) and ~850°C (848°C ± 6°C, 1SD), respectively. The temperature of the SC shows a wide range, from 800°C to 1100°C (897°C ± 99°C, 1SD), which may be reflected by pseudo-equilibrium during syn- or post-eruption. We assume that the eruption temperature of the SC is ~950°C based on an average value of the calculation results.

The chemical characteristics of pyroxene are shown in Supplementary Figure S2. No orthopyroxene (opx) within DP and few clinopyroxenes (cpx) within the SC were measured due to low contents (Table 1). Opx cores within WP and SC show Mg# [$100 \times Mg/(Mg + Fe)$] of 53 ± 7 (2SD, n = 45) and 59 ± 4 (2SD, n = 44), respectively. Most opx phenocrysts have cores with Mg# values that exceed that of each crystal's rims. The cpx cores within the SC and pre-CCFE basalt show Mg# of 63 (n = 1) and 76 ± 6 (n = 21, 2SD), respectively. By applying the cpx liquid thermometer (eq. 33 in the study by Putirka. (2008)), based on the mean chemical composition of the ground mass and the chemical composition of the cpx rims, the pre-CCFE basalt eruption temperature was estimated to be ~1100°C (1097°C ± 11°C, 1SD) (Supplementary Table S4). Olivine phenocrysts are only present within the pre-CCFE basalt.

5 Discussion

The three types of juvenile clast in the Aira CCFE deposits result from the corresponding three magmas, namely, rhyolite magma

FIGURE 7
Schematic representation of the formation processes of the three types of magmas in the Aira CCFE. Numbers in italics indicate $^{87}Sr/^{86}Sr$ values. Figures shown in wt% in each box represent SiO_2 contents.

(WP), rhyodacite magma (DP), and andesite magma (SC). Here, we discuss the petrogenesis of the three magmas.

The analytical results of the Sr-isotopic ratios in plagioclase phenocrysts and whole rock suggest that two source materials with distinct isotopic compositions explain the isotopic variation of the Aira CCFE magmas: one is a lower-$^{87}Sr/^{86}Sr$ material with $^{87}Sr/^{86}Sr$ of ~ 0.7055 and the other is a material with $^{87}Sr/^{86}Sr$ > 0.7086 (Figure 6A). The most voluminous magma in the Aira CCFE is the rhyolite magma, which occupies over 90% of the total volume. It has abundant low-An plagioclase phenocrysts with $^{87}Sr/^{86}Sr$ of 0.7055–0.7060, indicating that the main source material of the rhyolite magma is the low-$^{87}Sr/^{86}Sr$ material. However, the Sr isotopic and the An# variations of the WP plagioclases (Figure 6A) and high-An plagioclase phenocrysts from SC, whose Sr isotope ratios drastically change between 0.7055 and 0.7082, indicate interactions between isotopically different magmas.

For readability, we initially show our conceptual model od the magma plumbing system for the Aira CCFE (Figure 7). The main source material for Aira CCFE magmas is an amphibolite lower crust with ~0.7055 of $^{87}Sr/^{86}Sr$, and the anatexis of the amphibolite produced an original felsic magma with a low degree of partial melting and an original mafic magma with a high degree of partial melting. These original magmas evolved into the three magmas of the Aira CCFE (i.e., rhyolite, rhyodacite, and andesite) through various magmatic processes such as mixing, assimilation, and crystallization within the crust (Figure 7). They did not mix with basaltic magma derived from the mantle, which has a low $^{87}Sr/^{86}Sr$ (~0.7045) value.

To decode magma formation processes, trace element compositions of melts in equilibrium with plagioclase phenocrysts were estimated using the measured trace element concentrations of plagioclase and published plagioclase-melt element partition data (Bindeman et al., 1998; Bindeman and Davis, 2000). The melt compositions were calculated at assumed temperatures of 800°C and 950°C for <An_{64} and >An_{64} plagioclase, respectively, within the rhyolitic WP and andesitic SC, and 850°C was used for the plagioclase within the DP. All were inferred from the magmatic temperature for the Aira CCFE clasts based on ilmenite–magnetite thermometry (Ghiorso and Evans, 2008). The basalt temperature is estimated at 1100°C from the cpx-melt thermometer results. The parameters for the calculation and the results of partition coefficients and trace element compositions are listed in Supplementary Tables S5 and S6.

5.1 Origin of the original felsic and mafic magmas

The plagioclase cores are expected to record the geochemical characteristics of the original mafic and felsic magmas. Variations in An content and Sr-isotopic ratios in the plagioclase show that andesite and rhyolite magmas have experienced mixing processes with other components that have higher $^{87}Sr/^{86}Sr$ values (Figure 6A). However, the lowest $^{87}Sr/^{86}Sr$ values of the cores of the plagioclase phenocrysts in the rhyolite and andesite magmas are identical at ~0.7055. We judge this value as the $^{87}Sr/^{86}Sr$ values of the mafic and felsic magmas with little mixing influence. The agreement of the $^{87}Sr/^{86}Sr$ values in the mafic and felsic magmas implies that they are derived from the same source material. If mafic and felsic magmas are produced from the same source material, the source rock should have a mafic composition.

One presumable mafic source material is mantle-derived magma. If the source material is the mantle, basaltic to andesitic magmas should be produced first and then differentiated to produce dacitic to rhyolitic magmas. The basalt magmas that erupted in the Aira caldera have slightly higher $^{87}Sr/^{86}Sr$ values than those in southern Kyushu (Figure 3), and it was inferred that the fluid–mantle interaction resulted in geochemical variations of the mantle-derived basaltic magma (0.7039–0.7047) in this area (Shinjo et al., 2000). These values are within the range of mantle-derived xenoliths found in northern Kyushu (0.7042–0.7047; Senda et al., 2007), indicating that the pre-CCFE basalt magma was originally from the mantle. However, the lowest $^{87}Sr/^{86}Sr$ value of plagioclase cores (0.7054) is much higher than that in the basalt magma (Figure 6A), and the HREE concentrations of the rhyolite magma are lower than those of the basalt magma (Figure 2C). These observations indicate that simple fractional crystallization of the basalt magma cannot have produced the rhyolite magma in this case.

A strong possibility is that mantle-derived basaltic magma assimilated crustal rocks with higher $^{87}Sr/^{86}Sr$ values and differentiated, resulting in a change in the $^{87}Sr/^{86}Sr$ values from ~0.7045 to ~0.7055 and producing the Aira CCFE magma. However, the $^{87}Sr/^{86}Sr$ versus An# variations of the plagioclase within the Aira CCFE clasts (Figure 6A) indicate that this process may not be important in the formation of the Aira CCFE magma. We suggest that, if this process occurred, some traces of the

assimilation and fractional crystallization from the basaltic magma should be recorded in plagioclase cores, e.g., the presence of plagioclase with $^{87}Sr/^{86}Sr$ values of 0.7045–0.7055. However, as shown in Figure 6A, there is an isotopic gap between the plagioclase in the Aira CCFE clasts and in the mantle-derived basalt. Furthermore, in the low-An plagioclase within the Aira CCFE clasts, Sr isotopic ratios tend to be constant or slightly increase with increasing An#. Whereas we cannot categorically reject assimilation-fractional crystallization as a process, our data suggest that the mantle-derived basaltic magma did not contribute significantly to the mass of erupted magma. Therefore, the origin of rhyolite magma is most likely from crustal anatexis and not from assimilation–fractional crystallization.

Another plausible source material for the original mafic and felsic magmas is crustal rock. In this case, the low and high degrees of partial melting of the crustal rock would produce the original felsic and mafic magmas, respectively. Because the source material of the two magmas is assumed to be mafic in composition, the source is considered a deep crustal component (Rudnick and Gao, 2014). The model in which a large amount of magma that erupts in CCFEs is formed by melting crustal materials has been proposed in previous studies (Hildreth, 1981; de Silva, 2008; Kaneko et al., 2015), as well as a possible scenario in the Aira CCFEs (Arakawa et al., 1998; Takahashi et al., 2013; Kuritani, 2023). The crustal structure beneath the Aira caldera is estimated to have at least four layers in the crust (L1–L4 in order from upper to lower) with regions of different P-wave velocities (Ono et al., 1978). The uppermost crust at a depth of ~6 km below (L1 and L2) is interpreted to comprise the basement rocks such as granites and Shimanto Supergroup sediments (Miyamachi et al., 2013). However, these rocks are not the source material for Aira CCFEs' magmas because their Sr isotopic characteristics (>0.7086; Terakado et al., 1988; Hosono et al., 2003; Shin, 2008) are far from those of the original magmas (Figure 3; Figure 6A). The other candidates for the source materials are an upper crustal rock and a lower crustal rock (6–22 km and 22–40 km, respectively; Ono et al., 1978). Unfortunately, no xenoliths that can directly constrain the petrologic characteristics of these crustal rocks have been found in and around the Aira caldera, but a gabbro xenolith with $^{87}Sr/^{86}Sr$ value of 0.7054 has been found ~230 km north of the Aira caldera (Kagami et al., 1993). Furthermore, the presence of lower crustal materials with $^{87}Sr/^{86}Sr$ value of 0.705–0.706 has been proposed as one of the most plausible explanations for the whole-rock isotopic variations of the volcanic rocks that erupted in the vicinity of the Aira caldera (e.g., northwest area of the Aira caldera: Hosono et al., 2003; Hosono et al., 2008 and Aso caldera: Miyoshi et al., 2011).

To further constrain its origin, the REE signatures of the felsic magma are the key. In the whole rock compositions, the rhyolite magma is depleted in MREE and HREE (Figure 2C). To produce felsic magma of this nature, an amphibole or garnet contribution with high MREE-HREE compatibility must be involved in magma genesis. The small value of MREE/HREE, i.e., Dy/Yb of 1.5 calculated from the WP (Table 1), indicates that the amphibole is most likely responsible for the formation of the original felsic magma. Therefore, it is reasonable that the source rock of the Aira CCFE magmas is mafic amphibolite that comprises the lower crust.

To evaluate whether a partial melting of the amphibolite under lower crustal conditions could produce the original felsic magma, batch-melting calculations were conducted. The starting compositions of the mafic amphibolite were assumed to be identical to those of the pre-CCFE basalt (Table 1). To know the melt composition that could be formed by partial melting of the lower crust, model calculations of the partial melting process were performed based on the experimental results of the melting of lower crustal rocks (Springer and Seck, 1997). The residual phases at given degrees of partial melting (5% in Table 2) are based on experimental data of the metagabbro (S37), which has 7 vol% of amphibole and less garnet (1.5 vol%). The partition coefficients were adapted to the values based on the compiled values reported by Ewart and Griffin (1994), Rollinson (2014), Kimura et al. (2015), and Rollinson and Pease (2021) (Supplementary Table S7). For comparison of the original felsic magma composition with the modeling results, an average of the equilibrium melt compositions estimated from low An (<An$_{64}$) with the Sr-isotopic ratios of 0.7054–0.7060 was used. The results are listed in Table 2.

A systematic pattern of enrichment and depletion in certain elements can be observed for an inferred crustal amphibolite-derived felsic melt (Figure 8). After considering the crystal structure control on trace element partitioning between melts and crystals (Matsui et al., 1977; Wood and Blundy, 1997), this pattern suggests that the amphibolite-derived melt is more depleted in elements that are likely to be partitioned into amphibole and plagioclase, major constituent minerals in amphibolite. This can be understood to be the result of buffering of particular elements by residual phases during partial melting. The original felsic magma inferred from the element concentrations of plagioclase has a trace element pattern similar to that of the amphibolite-derived magma (Figure 8), which is consistent with the presence of amphibole and plagioclase during partial melting. This means that a small degree of the partial melting of the amphibolitic lower crust can explain the geochemical nature of the original felsic magma of the Aira CCFE. Therefore, the process for producing the original felsic and mafic magmas of the Aira CCFE was likely to be the melting of the mafic amphibolite.
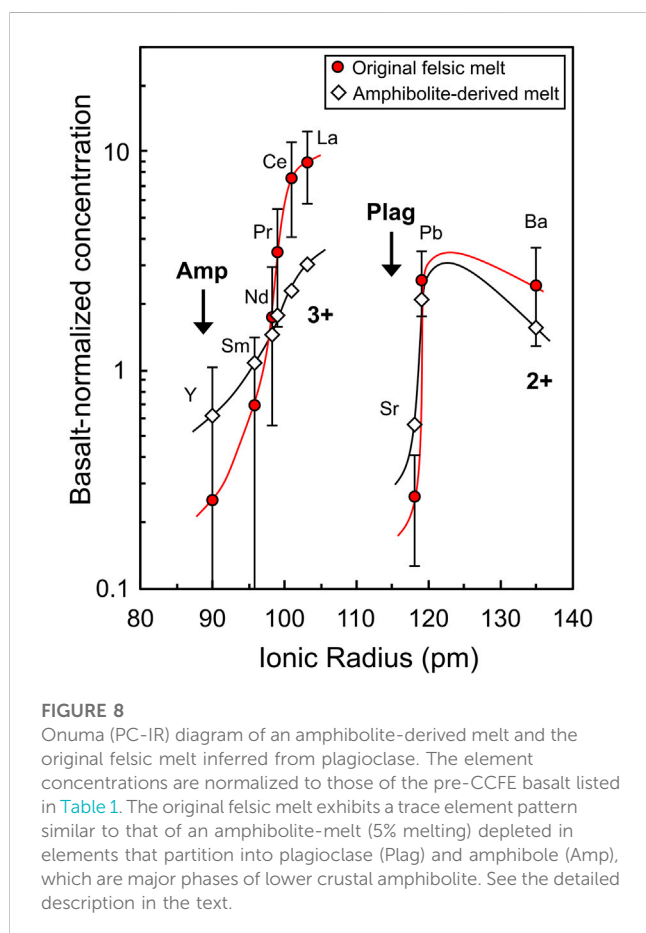
5.2 Petrogenesis of the three Aira magmas

As indicated at the beginning of this study, the three types of magmas corresponding to juvenile clasts in the Aira CCFE were generated by assimilation, mixing, and crystallization of the original felsic and mafic magmas within the uppermost crust. In the following section, we first clarify the formation process of the andesite magma that erupted as the SC, then the rhyolite magma that erupted as the WP, and finally, the rhyodacite magma that erupted as the DP.

5.2.1 Andesite magma

The andesite magma crystallized the plagioclase phenocrysts with remarkable features on the $^{87}Sr/^{86}Sr$ variation diagram (Figure 6). The Sr isotope ratios of the plagioclase increase as the An contents decrease and are higher at the plagioclase rims than at the cores. This suggests that the original mafic magma progressively assimilated high-$^{87}Sr/^{86}Sr$ material with crystallization. The most

TABLE 2 Compositions of the amphibolite-derived melt and the felsic melt from plagioclase.

Element	Amphibolite-derived melt			Inferred original felsic melt from plagioclase	
	Start (ppm)	Partition coefficient	5% melting (ppm)	Average (ppm)	1SD
Sr	349.3	1.80	198.4	93.3	25.4
Y	25.3	1.65	15.7	6.5	8.8
Ba	124.1	0.61	197.2	305.5	73.7
La	5.8	0.29	18.0	52.7	9.2
Ce	14	0.40	32.9	106.4	22.1
Pr	2.2	0.53	3.9	7.6	2.0
Nd	10.4	0.67	15.1	18.2	6.4
Sm	2.9	0.92	3.1	2.0	1.3
Pb	3.6	0.44	7.7	9.4	1.4

FIGURE 8
Onuma (PC-IR) diagram of an amphibolite-derived melt and the original felsic melt inferred from plagioclase. The element concentrations are normalized to those of the pre-CCFE basalt listed in Table 1. The original felsic melt exhibits a trace element pattern similar to that of an amphibolite-melt (5% melting) depleted in elements that partition into plagioclase (Plag) and amphibole (Amp), which are major phases of lower crustal amphibolite. See the detailed description in the text.

using the partition coefficient dataset for the intermediate composition reported by Ersoy and Helvacı (2010). The assimilant was estimated to be the published values of Shimanto sedimentary sediment rocks and Miocene granites (Sr of 148 ppm, La of 27 ppm, and $^{87}Sr/^{86}Sr$ of 0.71529) estimated from the published data (Terakado et al., 1988; Hosono et al., 2003; Shin. 2008). The assimilation/fractional crystallization rate (r value) is fixed at 0.6, the same as that reported by Arakawa et al. (1998). Here, partition coefficients for plagioclase were calculated for the crystallization of An_{90} and An_{70} at 950 °C (Bindeman et al., 1998) because the partition coefficients of the plagioclase, especially for Sr, drastically change as the AFC process progresses, i.e., the crystallizing An contents shift from high to low An. Furthermore, the Sr and La concentrations of the primitive mafic endmember melt were assumed to be 500 ppm and 3 ppm at $^{87}Sr/^{86}Sr$ of 0.7055, respectively. The fractional phases of the modeling are identical to those of the SC observed in the thin section (Table 1).

The calculation results in Figure 9 indicate that progressive AFC processes with changing partition coefficients can explain the geochemical variations of the inferred melt. Here, <~50% crystallization of the andesite magma could reproduce the inferred melt (Figure 9). The highest $^{87}Sr/^{86}Sr$ value observed in the plagioclase rim within the SC is 0.7082 ± 0.0002, suggesting the Sr isotopic ratio of melt of the andesite magma would have evolved to values above 0.7082 before the eruption. Although it is difficult to strictly constrain the chemical and isotopic heterogeneity of the andesite magma in the reservoir, this isotope range is important for elucidating the process of the formation of the rhyodacite magma (see Section 5.2.3).

5.2.2 Rhyolite magma

Petrographical and petrological observations suggest that mixing of a felsic magma with a small amount of the andesite magma formed the rhyolite magma (Figures 5, 6). The rhyolite magma has abundant low-An plagioclase phenocrysts and a small amount of high-An plagioclase phenocrysts. The low-An plagioclases have the same An contents as those of the felsic

likely assimilants with the isotopic characteristics around the Aira caldera are the sedimentary rocks and granite comprising the uppermost crust (see Section 5.1). Namely, the andesite magma of the Aira CCFE is derived from the original mafic magma that assimilated the uppermost crust and crystallized.

To evaluate this idea, AFC modeling was performed based on DePaolo (1981). The calculations were performed for Sr and La,
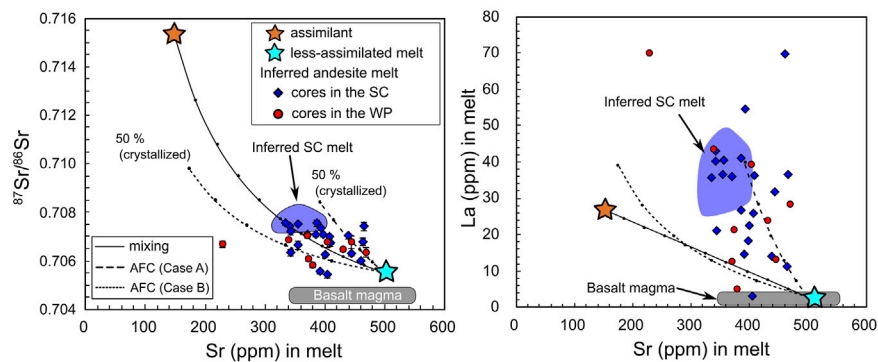
FIGURE 9
AFC and mixing calculation results of the mafic magma. The inferred andesite melt is the composition calculated from the high-An plagioclase core (>An$_{70}$) within the WP and SC and crystal-melt partition coefficient (Bindeman et al., 1998; Bindeman and Davis, 2000). The solid fields of the inferred SC melt and basalt magma are from the calculation results from the plagioclase rims within the SC and the plagioclase cores within the pre-CCFE basalt, respectively. Cases A and B (described as dashed and dotted lines, respectively) are the results in the case of the partition coefficients of plagioclase for An$_{90}$ (bulk D$_{Sr}$ = 0.74 and bulk D$_{La}$ = 0.143) and An$_{70}$ (bulk D$_{Sr}$ = 1.343 and bulk D$_{La}$ = 0.160), respectively. The solid cyan and orange stars represent assumed endmember compositions from the inferred andesite melt (Sr of 500 ppm, La of 3 ppm, and ^{87}Sr/^{86}Sr of 0.7055) and an average of the upper crustal rocks (Sr of 148 ppm, La of 27 ppm, and ^{87}Sr/^{86}Sr of 0.71529) reported by Terakado et al. (1988), Hosono et al. (2003), and Shin (2008), respectively. The solid line represents the simple mixing line between the two endmember compositions. The black dots on each line indicate intervals of every 10%. See detailed description in the text.

magma, and the high-An plagioclases have the same An contents and Sr-isotopic ratios as those of the andesitic SC.

To examine the mixing of the andesite and rhyolite magmas that reproduced the geochemical variations observed in Figure 6, a mixing calculation was performed. The mafic endmember components are estimated to be 0.7076 of ^{87}Sr/^{86}Sr and 348 ppm of Sr based on the average values of melt calculated from the plagioclase rims within the SC. The felsic endmember components are 0.7055 of ^{87}Sr/^{86}Sr and 88 ppm of Sr, which are from the low-An plagioclase with the lowest ^{87}Sr/^{86}Sr value observed in the WP. The mixing lines of the two endmember components are shown in Figure 10A.

The results of the calculation explain the chemical and isotopic variations observed in the rhyolite magma. The assumed mixing of the two endmember components can successfully account for the upper limit of geochemical variations that occurred during the formation of the rhyolite magma. This mixing line would correspond to the magma mixing at a relatively later period when the plagioclase rim was formed. In contrast, the melt compositions inferred from the plagioclase core are plotted below this mixing line, suggesting that the injection of andesitic magma into felsic magma accumulated within the upper crust occurred many times when the andesite magma had been less evolved, i.e., during the AFC process. Although it is difficult to constrain the mixing ratio of the two magmas because of the stepwise compositional changes of the andesite magma, Figure 10A suggests that approximately 10% of andesite magma (melt composition was dacitic) mixed with the original felsic magma (0.7055 of ^{87}Sr/^{86}Sr) to form the rhyolite magma. So, although Kimura et al. (2015) suggested that the source of the WP rhyolite is upper crustal granites based on the geochemical characteristics of the co-ignimbrite AT ash, we suggest here that mixing the rhyolite magma with the andesite magma changed the geochemical characteristics of the AT ash, i.e., the melt component of the rhyolite magma before the Aira CCFE.

Geshi et al. (2020) noticed that the temperature of the rhyolite magma discharged by the Osumi pumice fall is higher than that discharged by the pre-Aira CCFE activities at 60–31 ka. Furthermore, the rhyolite magmas discharged by eruptions during 60–30 ka have chemical compositions similar to those of the Aira CCFE, but the whole rock ^{87}Sr/^{86}Sr values of the rhyolite magmas discharged during 36 to 31 ka (0.7059–0.7060) are slightly higher than those of the 60-ka rhyolite magma (0.7055–0.7057) (Kuritani, 2023). Our model indicates that injection of the andesite magma into the rhyolite magma started at least 6,000 years before the Aira CCFE.

5.2.3 Rhyodacite magma

The rhyodacite magma was generated by mixing of the rhyolite magma and only the melt of the andesite magma. The andesite magma's liquid phase chemical composition before the eruption was rhyodacite (~70 wt% SiO$_2$), characterized by high HFSE concentrations. The mixing of the liquid phase of the andesite magma and the rhyolite magma can account for the compositional variations of the rhyodacitic magma (Figure 10B). Furthermore, this process can also explain the weak negative correlation with SiO$_2$ found in the LILE and HFSE of the rhyodacite magma (Figure 10B).

The assumption that only the liquid part of the andesite magma was mixed also follows the observation that the crystals in the rhyodacitic magma are mainly derived from the rhyolitic magma. No observation of plagioclase phenocrysts with the same Sr isotopic ratios as the rhyodacite magma (~0.7086) suggests that rhyodacite magma was formed on a short timescale before Aira CCFE precluding significant crystallization. This interpretation also follows the fact that DP, a solidification of rhyodacite magma, is mingled with the WP rhyolite magma.

Finally, we refer to the heterogeneity of the rhyodacite magma. As described above, the main process that led to the formation of the rhyodacite magma was the presence of andesitic magma formed
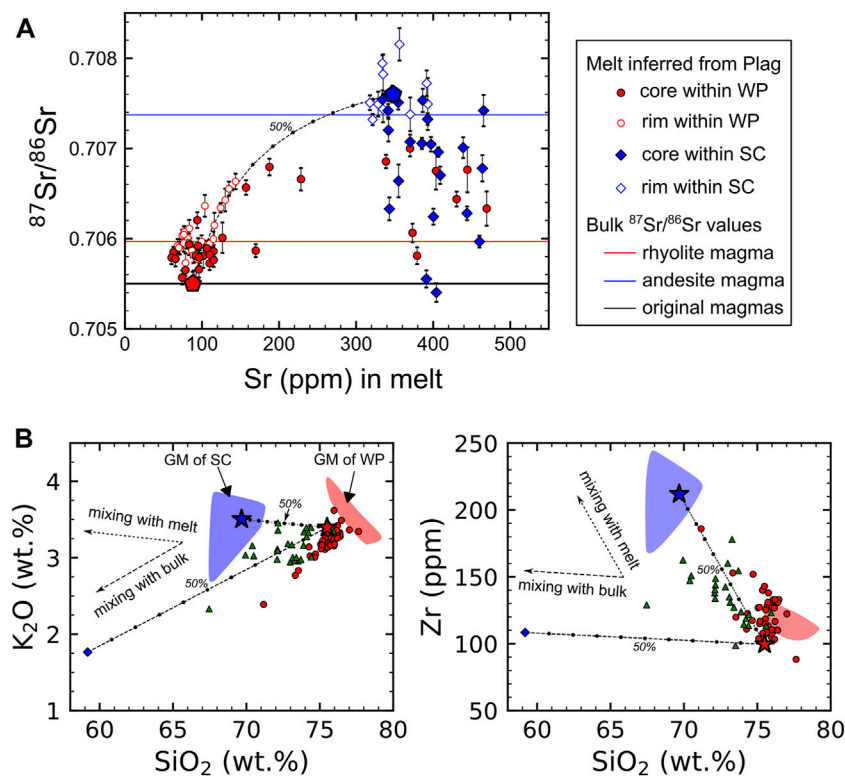
FIGURE 10
(A) Calculations of mixing of the felsic magma with the andesite magma. Red and blue horizontal lines represent whole-rock $^{86}Sr/^{86}Sr$ values of the rhyolite magma (WP) and the andesite magma (SC), respectively. The red and blue pentagons indicate the endmember compositions of the felsic and mafic components, respectively (see Section 5.2.2). The black dashed line is the mixed line, and the black dots on each line indicate intervals of every 10%. **(B)** DP formation models based on mixing calculations. Red and blue fields represent the groundmass glass (GM) of the WP and SC, respectively. The red star represents the WP (1608240602) in Table 1, and the blue star represents the average of the GM of the SC. The black dots on each line indicate intervals of every 10%.
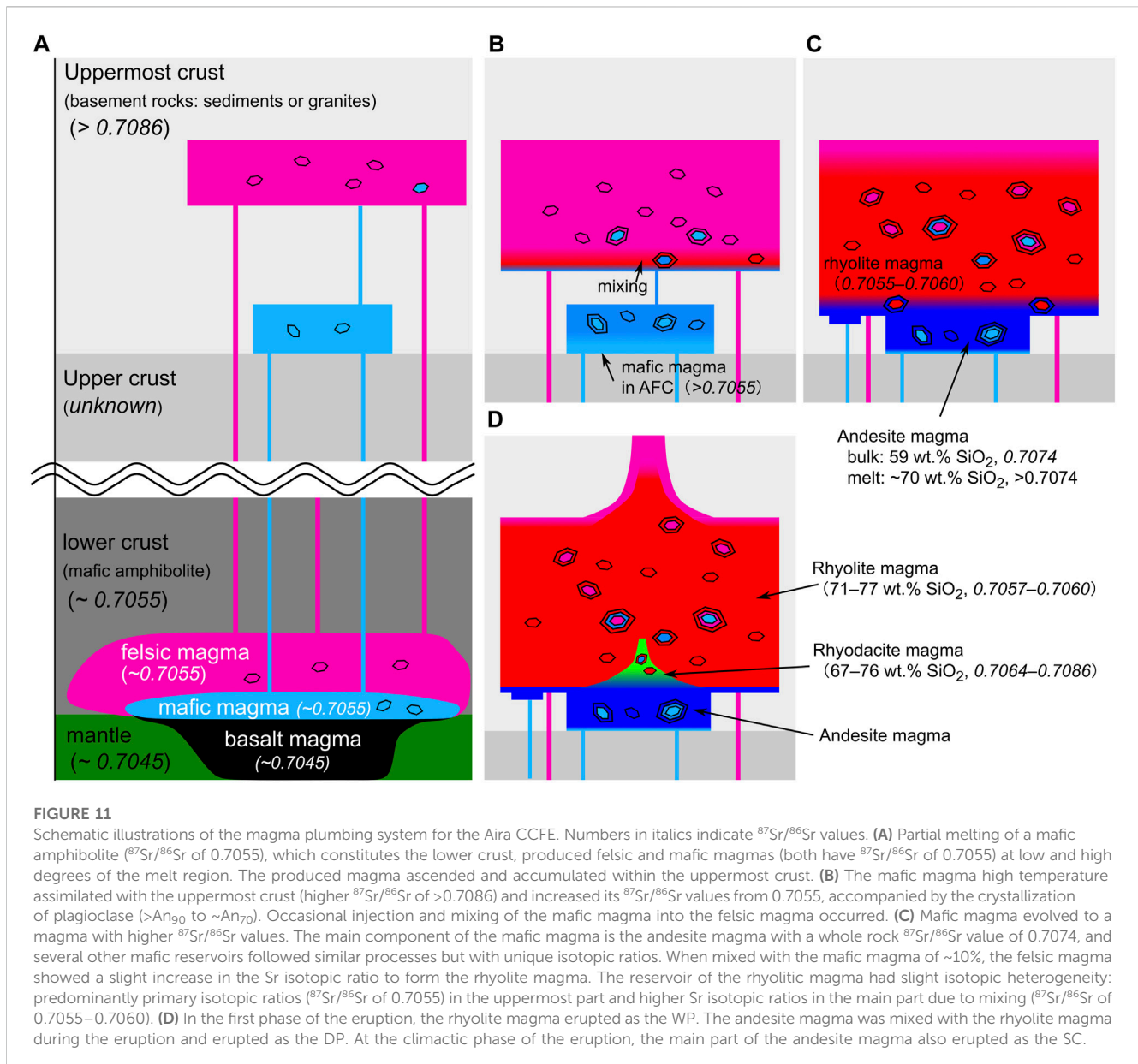
through crustal assimilation. However, DPs show broad ranges in chemical and isotopic compositions (Figures 2, 3) and sometimes have variable mineral assemblage (Tsukui and Aramaki, 1990). These observations indicate that the heterogeneity of the assimilant, i.e., uppermost crustal components beneath the Aira caldera, or the existence of multiple andesitic magma reservoirs existed before the Aira CCFE and the andesite and rhyolitic magmas might have mixed in various proportions. With the broad isotopic characteristic of the DPs, these observations may reflect the diversity of mafic magma reservoirs.

5.3 Magma plumbing system for the Aira CCFE

A schematic model for the magma plumbing system of the Aira CCFE is described in Figure 11. The heat source from the mantle melts the amphibolite lower crust with $^{87}Sr/^{86}Sr$ value of 0.7055, causing large-scale anataxis. The partially molten lower crust produced the original mafic magma in a highly partially molten region and the original felsic magma in the outer zone of the partially molten region with lower partial melting. Although a highly viscous silicic magma is hard to segregate from a partially molten zone, the

low strain rate in this tectonic setting may have increased the solid and melt viscosity contrast, enhancing segregation and upward migration of the rhyolite magma (Tatsumi and Suzuki-Kamata, 2014). Felsic magma accumulated in the upper crust, forming a huge magma reservoir. The mafic magma is also upwelled and stored at a relatively deeper level than the base of the rhyolite reservoir. The mafic magma with a higher temperature effectively assimilated the wall rocks composed of high-$^{87}Sr/^{86}Sr$ crust that may be either sediments or granites, obtained its higher $^{87}Sr/^{86}Sr$ values, and formed the andesite magma. It was injected into the bottom of the huge reservoirs and mixed with a felsic magma. Felsic magma mixing with the andesite magma produced the rhyolite magma, which further mixed with the andesite magma and produced the rhyodacite magma with various geochemical compositions.

This study reveals that the voluminous felsic magma erupted in the Aira CCFE, which was thought to be homogeneous high-silica rhyolite magma in terms of whole rock analysis, actually involved mixing with mafic magma based on Sr isotope variations in plagioclase. As summarized in the review by Wilson et al. (2021), the voluminous magmas involved in CCFEs are often derived from complex processes in the crust where multiple components are intermingled. This study could identify the formation process of multiple magmas that erupted in the CCFE, by elucidating the

FIGURE 11
Schematic illustrations of the magma plumbing system for the Aira CCFE. Numbers in italics indicate $^{87}Sr/^{86}Sr$ values. **(A)** Partial melting of a mafic amphibolite ($^{87}Sr/^{86}Sr$ of 0.7055), which constitutes the lower crust, produced felsic and mafic magmas (both have $^{87}Sr/^{86}Sr$ of 0.7055) at low and high degrees of the melt region. The produced magma ascended and accumulated within the uppermost crust. **(B)** The mafic magma high temperature assimilated with the uppermost crust (higher $^{87}Sr/^{86}Sr$ of >0.7086) and increased its $^{87}Sr/^{86}Sr$ values from 0.7055, accompanied by the crystallization of plagioclase (>An$_{90}$ to ~An$_{70}$). Occasional injection and mixing of the mafic magma into the felsic magma occurred. **(C)** Mafic magma evolved to a magma with higher $^{87}Sr/^{86}Sr$ values. The main component of the mafic magma is the andesite magma with a whole rock $^{87}Sr/^{86}Sr$ value of 0.7074, and several other mafic reservoirs followed similar processes but with unique isotopic ratios. When mixed with the mafic magma of ~10%, the felsic magma showed a slight increase in the Sr isotopic ratio to form the rhyolite magma. The reservoir of the rhyolitic magma had slight isotopic heterogeneity: predominantly primary isotopic ratios ($^{87}Sr/^{86}Sr$ of 0.7055) in the uppermost part and higher Sr isotopic ratios in the main part due to mixing ($^{87}Sr/^{86}Sr$ of 0.7055−0.7060). **(D)** In the first phase of the eruption, the rhyolite magma erupted as the WP. The andesite magma was mixed with the rhyolite magma during the eruption and erupted as the DP. At the climactic phase of the eruption, the main part of the andesite magma also erupted as the SC.

origins of the primitive magmas and their processes of interaction in the crust.

6 Conclusion

The 30-ka Aira CCFE discharged three types of magmas: rhyolite, rhyodacite, and andesite magmas. The three magmas comprised felsic magma and mafic magma generated by partial melting of the lower crust, which underwent mixing, crystallization, and assimilation within the crusts to form the erupted magma.

The main source material of the Aira CCFE magmas is the mafic amphibolite lower crust with a low $^{87}Sr/^{86}Sr$ (~0.7055) value. The lower crust produced felsic and mafic magmas via low and high degrees of partial melting, respectively. The felsic and mafic magmas generated in the lower crust ascended to the uppermost crust and formed magma chambers. The mafic magma in the chamber

assimilated with the wall rock and crystallized, forming andesite magma that was the source of SC. Injections of the andesite magma (~10%) into the felsic magma (~90%) in the uppermost crustal magma reservoir and crystallization produced the rhyolite magma, producing the WP. Mixing of the dacitic liquid of the andesite magma and the rhyolite magma before the eruption produced the rhyodacite magma that erupted as the DP.

This study reveals that the 30-ka Aira CCFE magmas were generated only by melting two kinds of crustal materials with different geochemical characteristics and had geochemical variations in different conditions of partial melting and mixing between various crustal melts. The lack of definitive evidence that the mantle component mixed with the Aira CCFE magmas suggests that the mantle-derived magmas worked only as a heat source for crustal melting. This study is a good example of how the Aira CCFE was caused by magma produced by crustal melting and how complex processes within the crust were identified to understand the origin of the source magma. Applying the methods of this study to other

volcanoes will help in better understanding the nature of magma formation processes that cause CCFEs.

Data availability statement

The original contributions presented in the study are included in the article/Supplementary Material; further inquiries can be directed to the corresponding author.

Author contributions

Funding

Acknowledgments

Conflict of interest

Publisher's note

Supplementary material

The Supplementary Material for this article can be found online at: https://www.frontiersin.org/articles/10.3389/feart.2023.1283844/full#supplementary-material

References

Annen, C., Blundy, J. D., and Sparks, R. S. J. (2006). The genesis of intermediate and silicic magmas in deep crustal hot zones. J. Petrol. 47 (3), 505–539. doi:10.1093/petrology/egi084

Arakawa, Y., Kurosawa, M., Takahashi, K., Kobayashi, Y., Tsukui, M., and Amakawa, H. (1998). Sr–Nd isotopic and chemical characteristics of the silicic magma reservoir of the Aira pyroclastic eruption, southern Kyushu, Japan. J. Volcanol. Geotherm. Res. 80 (3), 179–194. doi:10.1016/S0377-0273(97)00046-2

Aramaki, S. (1969). Geology and pyroclastic flow deposits of the Kokubu area, Kagoshima Prefecture. J. Geol. Soc. Jpn. 75 (8), 425–442. doi:10.5575/geosoc.75.425

Aramaki, S. (1984). Formation of the Aira caldera, southern Kyushu, ~22,000 years ago. J. Geophys. Res. Solid Earth 89 (B10), 8485–8501. doi:10.1029/JB089iB10p08485

Bachmann, O., and Bergantz, G. (2008). The magma reservoirs that feed supereruptions. Elements 4 (1), 17–21. doi:10.2113/GSELEMENTS.4.1.17

Bacon, C. R., and Hirschmann, M. M. (1988). Mg/Mn partitioning as a test for equilibrium between coexisting Fe-Ti oxides. Am. Mineral. 73 (1-2), 57–61.

Bindeman, I. N., and Davis, A. M. (2000). Trace element partitioning between plagioclase and melt: investigation of dopant influence on partition behavior. Geochim. Cosmochim. Acta 64 (16), 2863–2878. doi:10.1016/s0016-7037(00)00389-6

Bindeman, I. N., Davis, A. M., and Drake, M. J. (1998). Ion microprobe study of plagioclase-basalt partition experiments at natural concentration levels of trace elements. Geochim. Cosmochim. Acta 62 (7), 1175–1193. doi:10.1016/s0016-7037(98)00047-7

Chang, Q., Kimura, J.-I., and Vaglarov, B. S. (2015). In situ Sr isotope measurement of small glass samples using multiple-Faraday collector inductively coupled plasma mass spectrometry with 10 12 Ω resistor high gain Faraday amplifiers. J. Anal. At. Spectrom. 30 (2), 515–524. doi:10.1039/c4ja00297k

Chang, Q., Shibata, T., Shinotsuka, K., Yoshikawa, M., and Tatsumi, Y. (2003). Precise determination of trace elements in geological standard rocks using inductively coupled plasma mass spectrometry (ICP-MS). Front. Res. Earth Evol. 1, 357–362.

Charlier, B. L. A., Wilson, C. J. N., and Davidson, J. P. (2008). Rapid open-system assembly of a large silicic magma body: time-resolved evidence from cored plagioclase crystals in the Oruanui eruption deposits, New Zealand. Contrib. Mineral. Petrol. 156 (6), 799–813. doi:10.1007/s00410-008-0316-y

Davidson, J. P., Morgan, D. J., Charlier, B. L. A., Harlou, R., and Hora, J. M. (2007). Microsampling and isotopic analysis of igneous rocks: implications for the study of magmatic systems. Annu. Rev. Earth Planet. Sci. 35 (1), 273–311. doi:10.1146/annurev.earth.35.031306.140211

DePaolo, D. J. (1981). Trace element and isotopic effects of combined wallrock assimilation and fractional crystallization. Earth Planet. Sci. Lett. 53 (2), 189–202. doi:10.1016/0012-821X(81)90153-9

de Silva, S. (2008). Arc magmatism, calderas, and supervolcanoes. Geology 36 (8), 671–672. doi:10.1130/focus082008.1

Ersoy, Y., and Helvacı, C. (2010). FC–AFC–FCA and mixing modeler: a Microsoft® Excel© spreadsheet program for modeling geochemical differentiation of magma by crystal fractionation, crustal assimilation and mixing. Comput. Geosci. 36 (3), 383–390. doi:10.1016/j.cageo.2009.06.007

Ewart, A., and Griffin, W. L. (1994). Application of proton-microprobe data to trace-element partitioning in volcanic rocks. Chem. Geol. 117 (1), 251–284. doi:10.1016/0009-2541(94)90131-7

Fukushima, D., and Kobayashi, T. (2000). Mechanism of generation and emplacement of the tarumizu pyroclastic flow associated with Osumi plinian eruption from Aira caldera, Japan. Bull. Volcanol. Soc. Jpn. 45 (4), 225–240. doi:10.18940/kazan.45.4_225

Geshi, N., and Miyabuchi, Y. (2016). Conduit enlargement during the precursory plinian eruption of Aira caldera, Japan. *Bull. Volcanol.* 78 (9), 63. doi:10.1007/s00445-016-1057-9

Geshi, N., Yamada, I., Matsumoto, K., Nishihara, A., and Miyagi, I. (2020). Accumulation of rhyolite magma and triggers for a caldera-forming eruption of the Aira Caldera, Japan. *Bull. Volcanol.* 82 (6), 44–18. doi:10.1007/s00445-020-01384-6

Geshi, N., Yamasaki, T., Miyagi, I., and Conway, C. E. (2021). Magma chamber decompression during explosive caldera-forming eruption of Aira caldera. *Commun. Earth Environ.* 2 (1), 200. doi:10.1038/s43247-021-00272-x

Ghiorso, M. S., and Evans, B. W. (2008). Thermodynamics of rhombohedral oxide solid solutions and a revision of the Fe-Ti two-oxide geothermometer and oxygen-barometer. *Am. J. Sci.* 308 (9), 957–1039. doi:10.2475/09.2008.01

Hildreth, W. (1981). Gradients in silicic magma chambers: implications for lithospheric magmatism. *J. Geophys. Res. Solid Earth* 86 (B11), 10153–10192. doi:10.1029/JB086iB11p10153

Hirahara, Y., Chang, Q., Miyazaki, T., Takahashi, T., and Kimura, J.-I. (2012). Improved Nd chemical separation technique for 143Nd/144Nd analysis in geological samples using packed Ln resin columns. *JAMSTEC Rep. Res. Dev.* 15, 27–33. doi:10.5918/jamstecr.15.27

Hosono, T., Nakano, T., and Murakami, H. (2003). Sr–Nd–Pb isotopic compositions of volcanic rocks around the Hishikari gold deposit, southwest Japan: implications for the contribution of a felsic lower crust. *Chem. Geol.* 201 (1-2), 19–36. doi:10.1016/s0009-2541(03)00205-5

Hosono, T., Nakano, T., Shin, K., and Murakami, H. (2008). Assimilation of lower to middle crust by high alumina basalt magma as an explanation for the origin of medium-K volcanic rocks in southern Kyushu, Japan. *Lithos* 105 (1), 51–62. doi:10.1016/j.lithos.2008.02.007

Inoue, H., Itaya, T., and Tatsumi, Y. (1994). Petrography, K-Ar age, and chemistry of Yoshino-dai lavas in the Aira caldera. *Bull. Disaster Prev. Res. Inst.* 44 (4), 175–190. Avaliable at: http://hdl.handle.net/2433/125006.

Jochum, K. P., Willbold, M., Raczek, I., Stoll, B., and Herwig, K. (2005). Chemical characterisation of the USGS reference glasses GSA-1G, GSC-1G, GSD-1G, GSE-1G, BCR-2G, BHVO-2G and BIR-1G using EPMA, ID-TIMS, ID-ICP-MS and LA-ICP-MS. *Geostand. Geoanal. Res.* 29 (3), 285–302. doi:10.1111/j.1751-908X.2005.tb00901.x

Jones, G. S., Gregory, J. M., Stott, P. A., Tett, S. F. B., and Thorpe, R. B. (2005). An AOGCM simulation of the climate response to a volcanic super-eruption. *Clim. Dyn.* 25 (7-8), 725–738. doi:10.1007/s00382-005-0066-8

Kagami, H., Iizumi, S., Iwata, M., and Nureki, T. (1993). Sr-Nd isotope systematics of xenoliths in cenozoic volcanic rocks from SW Japan. *Proc. Jpn. Acad. Ser. B* 69 (1), 1–6. doi:10.2183/pjab.69.1

Kagawa, A., and Otsuka, H. (2000). Stratigraphic sequence and volcano-tectonic event deposits of the middle Pleistocene Kokubu Group on the coastal area of the north Kagoshima Bay, South Kyushu, Japan. *J. Geol. Soc. Jpn.* 106 (11), 762–782. doi:10.5575/geosoc.106.762

Kaneko, K., Inoue, K., Koyaguchi, T., Yoshikawa, M., Shibata, T., Takahashi, T., et al. (2015). Magma plumbing system of the Aso-3 large pyroclastic eruption cycle at Aso volcano, Southwest Japan: petrological constraint on the formation of a compositionally stratified magma chamber. *J. Volcanol. Geotherm. Res.* 303, 41–58. doi:10.1016/j.jvolgeores.2015.07.016

Kaneoka, I., Aramaki, S., Kobayashi, T., and Oki, K. (1984). Pliocene and Pleistocene volcanism in southern Kyushu: K-Ar ages of fumoto and isaku pyroclastic flows and related rocks. *SECOND Ser. Bull. Volcanol. Soc. Jpn.* 29 (1), 59–62. doi:10.18940/kazanc.29.1_59

Kimura, J.-I., and Chang, Q. (2012). Origin of the suppressed matrix effect for improved analytical performance in determination of major and trace elements in anhydrous silicate samples using 200 nm femtosecond laser ablation sector-field inductively coupled plasma mass spectrometry. *J. Anal. At. Spectrom.* 27 (9), 1549–1559. doi:10.1039/c2ja10344c

Kimura, J.-I., Nagahashi, Y., Satoguchi, Y., and Chang, Q. (2015). Origins of felsic magmas in Japanese subduction zone: geochemical characterizations of tephra from caldera-forming eruptions <5 Ma. *Geochem. Geophys. Geosyst.* 16 (7), 2147–2174. doi:10.1002/2015gc005854

Kimura, J.-I., Takahashi, T., and Chang, Q. (2013). A new analytical bias correction for *in situ* Sr isotope analysis of plagioclase crystals using laser-ablation multiple-collector inductively coupled plasma mass spectrometry. *J. Anal. At. Spectrom.* 28 (6), 945–957. doi:10.1039/C3JA30329B

Kita, I., Asakawa, Y., Yuri, T., Yasui, M., Shimoike, Y., Yamamoto, M., et al. (2012). Rifting of Kyushu, Japan, based on the fault-controlled concurrent eruption of oceanic island basalt-type and island arc-type lavas. *Bull. Volcanol.* 74 (5), 1121–1139. doi:10.1007/s00445-012-0587-z

Kobayashi, T., Hayakawa, Y., and Aramaki, S. (1983). Thickness and grain-size distribution of the Osumi pumice fall deposit from the Aira caldera. *SECOND Ser. Bull. Volcanol. Soc. Jpn.* 28 (2), 129–139. doi:10.18940/kazanc.28.2_129

Koornneef, J. M., Bouman, C., Schwieters, J. B., and Davies, G. R. (2013). Use of 10 12 ohm current amplifiers in Sr and Nd isotope analyses by TIMS for application to sub-nanogram samples. *J. Anal. At. Spectrom.* 28 (5), 749–754. doi:10.1039/c3ja30326h

Kurasawa, H., Arai, F., and Machida, H. (1984). Strontium isotopic identification of the widespread aira-tn ash-fall deposits (AT) in Japan. *SECOND Ser. Bull. Volcanol. Soc. Jpn.* 29 (2), 115–118. doi:10.18940/kazanc.29.2_115

Kuritani, T. (2023). Geochemical constraints on the evolution of the magmatic system leading to catastrophic eruptions at Aira Caldera, Japan. *Lithos* 450–451, 107208. doi:10.1016/j.lithos.2023.107208

Le Bas, M. J., Le Maitre, R. W., Streckeisen, A., and Zanettin, B. (1986). A chemical classification of volcanic rocks based on the total alkali-silica diagram. *J. Petrol.* 27 (3), 745–750. doi:10.1093/petrology/27.3.745

Le Maitre, R. W., Streckeisen, A., Zanettin, B., Le Bas, M. J., Bonin, B., and Bateman, P. (2002). *Igneous rocks: a classification and glossary of terms: recommendations of the international union of geological sciences subcommission on the systematics of igneous rocks.* Cambridge: Cambridge University Press. doi:10.1017/CBO9780511535581

Machida, H., and Arai, F. (1976). The widespread tephra — the Aira-Tn ash. *Kagaku* 46 (6), 339–347.

Machida, H., and Arai, F. (1983). Extensive ash falls in and around the sea of Japan from large late quaternary eruptions. *J. Volcanol. Geotherm. Res.* 18 (1), 151–164. doi:10.1016/0377-0273(83)90007-0

Matsui, Y., Onuma, N., Nagasawa, H., Higuchi, H., and Banno, S. (1977). Crystal structure control in trace element partition between crystal and magma. *Bull. Mineral.* 100 (6), 315–324. doi:10.3406/bulmi.1977.7155

Matumoto, T. (1943). The four gigantic caldera volcanoes of Kyushu. *Jpn. J. Geol. Geog.* 19, 1–57.

Miyamachi, H., Tomari, C., Yakiwara, H., Iguchi, M., Tameguri, T., Yamamoto, K., et al. (2013). Shallow velocity structure beneath the Aira caldera and Sakurajima volcano as inferred from refraction analysis of the seismic experiment in 2008(<Special Section>Sakurajima special issue). *Bull. Volcanol. Soc. Jpn.* 58 (1), 227–237. doi:10.18940/kazan.58.1_227

Miyazaki, T., Hanyu, T., Kimura, J.-I., Senda, R., Vaglarov, B. S., Chang, Q., et al. (2018). Clinopyroxene and bulk rock Sr–Nd–Hf–Pb isotope compositions of Raivavae ocean island basalts: does clinopyroxene record early stage magma chamber processes? *Chem. Geol.* 482, 18–31. doi:10.1016/j.chemgeo.2017.12.015

Miyazaki, T., Vaglarov, B. S., Takei, M., Suzuki, M., Suzuki, H., Ohsawa, K., et al. (2012). Development of a fully automated open-column chemical-separation system—COLUMNSPIDER—and its application to Sr-Nd-Pb isotope analyses of igneous rock samples. *J. Mineral. Petrol. Sci.* 107 (2), 74–86. doi:10.2465/jmps.110520

Miyoshi, M., Shibata, T., Yoshikawa, M., Sano, T., Shinmura, T., and Hasenaka, T. (2011). Genetic relationship between post-caldera and caldera-forming magmas from Aso volcano, SW Japan: constraints from Sr isotope and trace element compositions. *J. Mineral. Petrol. Sci.* 106 (2), 114–119. doi:10.2465/jmps.101021b

Nagaoka, S., Okuno, M., and Arai, F. (2001). Tephrostratigraphy and eruptive history of the Aira caldera volcano during 100-30 ka, Kyushu, Japan. *J. Geol. Soc. Jpn.* 107 (7), 432–450. doi:10.5575/geosoc.107.432

Newhall, C., Self, S., and Robock, A. (2018). Anticipating future Volcanic Explosivity Index (VEI) 7 eruptions and their chilling impacts. *Geosphere* 14 (2), 572–603. doi:10.1130/GES01513.1

Nishizawa, F., and Suzuki, T. (2020). Characterization and correlation of the Hegawa-Kasamori 5 tephra, a widespread tephra aged c. 450 ka associated with large-scale pyroclastic flows from southern Kyushu, SW Japan. *J. Quat. Sci.* 35 (1-2), 288–303. doi:10.1002/jqs.3172

Oki, K., and Hayasaka, S. (1970). Quaternary stratigraphy in the northern part of kagoshima city. *Earth Sci. Biol.* 3, 67–92. Avaliable at: http://hdl.handle.net/10232/5851.

Ono, K., Ito, K., Hasegawa, I., Ichikawa, K., Iizuka, S., Kakuta, T., et al. (1978). EXPLOSION SEISMIC STUDIES IN SOUTH KYUSHU ESPECIALLY AROUND THE SAKURAJIMA VOLCANO. *J. Phys. Earth* 26, S309–S319. doi:10.4294/jpe1952.26.Supplement_S309

Putirka, K. D. (2008). Thermometers and barometers for volcanic systems. *Rev. Mineral. Geochem.* 69 (1), 61–120. doi:10.2138/rmg.2008.69.3

Rampino, M. R., and Self, S. (1992). Volcanic winter and accelerated glaciation following the Toba super-eruption. *Nature* 359 (6390), 50–52. doi:10.1038/359050a0

Rampino, M. R., Self, S., and Stothers, R. B. (1988). Volcanic winters. *Annu. Rev. Earth Planet. Sci.* 16 (1), 73–99. doi:10.1146/annurev.ea.16.050188.000445

Rollinson, H. R. (2014). *Using geochemical data: evaluation, presentation, interpretation.* London: Routledge.

Rollinson, H., and Pease, V. (2021). *Using geochemical data to understand geological processes.* Cambridge University Press.

Rudnick, R. L., and Gao, S. (2014). "4.1 - composition of the continental crust," in *Treatise on geochemistry*. Editors H. D. Holland and K. K. Turekian (Elsevier), 1–51. doi:10.1016/B978-0-08-095975-7.00301-6

Sas, M., Shane, P., Kuritani, T., Zellmer, G. F., Kent, A. J. R., and Nakagawa, M. (2021). Mush, melts and metasediments: a history of rhyolites from the okataina volcanic centre, New Zealand, as captured in plagioclase. *J. Petrol.* 62 (8), egab038. doi:10.1093/petrology/egab038

Senda, R., Tanaka, T., and Suzuki, K. (2007). Os, Nd, and Sr isotopic and chemical compositions of ultramafic xenoliths from Kurose, SW Japan: implications for contribution of slab-derived material to wedge mantle. *Lithos* 95 (3-4), 229–242. doi:10.1016/j.lithos.2006.07.014

Shibata, T., Suzuki, J., Yoshikawa, M., Kobayashi, T., Miki, D., and Takemura, K. (2013). Geochemical and Sr-Nd-Pb isotopic constraints on the origin and magmatic evolution of quaternary lavas of Sakurajima volcano, southern Kyushu island, Japan(<Special Section>Sakurajima special issue). *Bull. Volcanol. Soc. Jpn.* 58 (1), 43–58. doi:10.18940/kazan.58.1_43

Shin, K. (2008). Geochemical study of the back arc Tsushima granite pluton and its comparison to the other Middle Miocene granites in southwest Japan. Ph.D Thesis. Japan: University of Tsukuba.

Shinjo, R., Woodhead, J. D., and Hergt, J. M. (2000). Geochemical variation within the northern Ryukyu Arc: magma source compositions and geodynamic implications. *Contrib. Mineral. Petrol.* 140 (3), 263–282. doi:10.1007/s004100000191

Smith, V. C., Staff, R. A., Blockley, S. P. E., Bronk Ramsey, C., Nakagawa, T., Mark, D. F., et al. (2013). Identification and correlation of visible tephras in the Lake Suigetsu SG06 sedimentary archive, Japan: chronostratigraphic markers for synchronising of east Asian/west Pacific palaeoclimatic records across the last 150 ka. *Quat. Sci. Rev.* 67, 121–137. doi:10.1016/j.quascirev.2013.01.026

Springer, W., and Seck, H. A. (1997). Partial fusion of basic granulites at 5 to 15 kbar: implications for the origin of TTG magmas. *Contrib. Mineral. Petrol.* 127 (1), 30–45. doi:10.1007/s004100050263

Sudo, M., Ishihara, K., and Tatsumi, Y. (2000a). Pre-caldera volcanic history in Aira caldera area: K-Ar dating of lavas from kajiki and kokubu areas in northern part and ushine area in southern part of the caldera. *Bull. Volcanol. Soc. Jpn.* 45 (1), 1–12. doi:10.18940/kazan.45.1_1

Sudo, M., Uto, K., Miki, D., and Ishihara, K. (2001). K-Ar dating of volcanic rocks along the Aira caldera rim: Part 2: volcanic history of western and northwestern area of caldera and Sakurajima volcano. *Annu. Disas, Prev. Res. Inst. Kyoto Univ.* 44, 305–316. Avaliable at: http://hdl.handle.net/2433/80514.

Sudo, M., Uto, K., Miki, D., Ishihara, K., and Tatsumi, Y. (2000b). K-Ar dating of volcanic rocks along the Aira caldera rim - volcanic history before explosive Aira pyroclastic eruption -. *Annu. Disas, Prev. Res. Inst., Kyoto Univ.* 43 (B-1), 15–35. Avaliable at: http://hdl.handle.net/2433/80463.

Sun, S. s., and McDonough, W. F. (1989). Chemical and isotopic systematics of oceanic basalts: Implications for mantle composition and processes. *Geol. Soc. Lond. Spec. Publ.* 42 (1), 313. doi:10.1144/GSL.SP.1989.042.01.19

Takahashi, M., Otsuka, T., Kawamata, H., Sako, H., Yasui, M., Kanamaru, T., et al. (2011). Whole-rock chemistry for eruptive products of the Sakurajima volcano and Aira caldera, southern Kyushu: summary of 583 analytical data. *Proc. Inst. Nat. Sci. Nihon Univ. Sect. II, Dep. Geosystem Sci.* 46, 133–200.

Takahashi, M., Otsuka, T., Sako, H., Kawamata, H., Yasui, M., Kanamaru, T., et al. (2013). Temporal variation for magmatic chemistry of the Sakurajima volcano and Aira caldera region, southern Kyushu, southwest Japan since 61 ka and its implications for the evolution of magma chamber system (< special Section> Sakurajima special issue). *Bull. Volcanol. Soc. Jpn.* 58 (1), 19–42. doi:10.18940/kazan.58.1_19

Takahashi, T., Hirahara, Y., Miyazaki, T., Vaglarov, B. S., Chang, Q., Kimura, J.-i., et al. (2009). Precise determination of Sr isotope ratios in igneous rock samples and application to micro-analysis of plagioclase phenocrysts. *JAMSTEC Rep. Res. Dev.* 2009, 59–64. doi:10.5918/jamstecr.2009.59

Takarada, S., Nishihara, A., Hoshizumi, H., Yamasaki, T., Kaneda, Y., and Geshi, N. (2022). *Distribution map of Ito ignimbrite and associated deposits, Aira caldera, Japan.* Tsukuba: Geological Survey of Japan, AIST. Available at: https://www.gsj.jp/inquiryEN.html.

Tanaka, T., Togashi, S., Kamioka, H., Amakawa, H., Kagami, H., Hamamoto, T., et al. (2000). JNdi-1: a neodymium isotopic reference in consistency with LaJolla neodymium. *Chem. Geol.* 168 (3-4), 279–281. doi:10.1016/s0009-2541(00)00198-4

Tatsumi, Y., and Suzuki-Kamata, K. (2014). Cause and risk of catastrophic eruptions in the Japanese Archipelago. *Proc. Jpn. Acad. Ser. B* 90 (9), 347–352. doi:10.2183/pjab.90.347

Terakado, Y., Shimizu, H., and Masuda, A. (1988). Nd and Sr isotopic variations in acidic rocks formed under a peculiar tectonic environment in Miocene Southwest Japan. *Contrib. Mineral. Petrol.* 99 (1), 1–10. doi:10.1007/bf00399360

Tsukui, M., and Aramaki, S. (1990). The magma reservoir of the Aira pyroclastic eruption: a remarkably homogeneous high-silica rhyolite magma reservoir. *SECOND Ser. Bull. Volcanol. Soc. Jpn.* 35 (2), 231–248. doi:10.18940/kazanc.35.2_231

Ueno, T. (2007). Feature and formation mechanism of lithic fragment concentration zone of the Ito pyroclastic flow deposit, Aira Caldera, Japan. *Proc. Inst. Nat. Sci. Nihon Univ.* 42, 129–147.

Ueno, T. (2016). Features, source, and eruption volume of the Tsumaya pyroclastic flow deposit of the Aira caldera, southern Kyushu, Japan. *Bull. Volcanol. Soc. Jpn.* 61 (3), 533–544. doi:10.18940/kazan.61.3_533

Wallis, S. R., Yamaoka, K., Mori, H., Ishiwatari, A., Miyazaki, K., and Ueda, H. (2020). The basement geology of Japan from A to Z. *Isl. Arc* 29 (1), e12339. doi:10.1111/iar.12339

Wilson, C. J. N., Cooper, G. F., Chamberlain, K. J., Barker, S. J., Myers, M. L., Illsley-Kemp, F., et al. (2021). No single model for supersized eruptions and their magma bodies. *Nat. Rev. Earth Environ.* 2 (9), 610–627. doi:10.1038/s43017-021-00191-7

Wood, B. J., and Blundy, J. D. (1997). A predictive model for rare earth element partitioning between clinopyroxene and anhydrous silicate melt. *Contrib. Mineral. Petrol.* 129 (2), 166–181. doi:10.1007/s004100050330